# Discovery of Enaminone-Linked Benzofuran Derivatives as Dual VEGFR-2/hCA IX Inhibitors Exhibiting Hypoxia-Mediated Chemosensitization

Wagdy M. Eldehna[1,*] Zainab M. Elsayed[2], Mohamed R. Elnagar[3,4], Andrea Ammara[5], Mahmoud S. Elkotamy[6], Rehan Monir[7], Alessio Nocentini[5], Mohammed M. Al-Sanea[8], Claudiu T. Supuran[5], Haytham O. Tawfik[9,*] Hatem A. Abdel-Aziz[10], Ahmed T. Negmeldin [11,12]

[1] *Department of Pharmaceutical Chemistry, Faculty of Pharmacy, Kafrelsheikh University, P.O. Box 33516, Kafrelsheikh, Egypt.*

[2] *Scientific Research and Innovation Support Unit, Faculty of Pharmacy, Kafrelsheikh University, Kafrelsheikh 33516, Egypt.*

[3] *Department of Pharmacology and Toxicology, Faculty of Pharmacy, Al-Azhar University, Cairo 11823, Egypt.*

[4] *Department of Pharmacology, College of Pharmacy, The Islamic University, Najaf 54001, Iraq.*

[5] *Department of NEUROFARBA, Section of Pharmaceutical and Nutraceutical Sciences, University of Florence, Polo Scientifico, Via U. Schiff 6, 50019, Sesto Fiorentino, Firenze, Italy.*

[6] *Department of Pharmaceutical Chemistry, Faculty of Pharmacy, Alsalam University, Kafr El Zayat, 31611, El Gharbeia, Egypt.*

[7] *Clinical Biochemistry Department, College of Medicine, King Khalid University, Asir 61421, Saudi Arabia.*

[8] *Department of Pharmaceutical Chemistry, College of Pharmacy, Jouf University, Sakaka, Aljouf 72388, Saudi Arabia.*

[9] *Department of Pharmaceutical Chemistry, Faculty of Pharmacy, Tanta University, Tanta, 31527, Egypt.*

[10] *Applied Organic Chemistry Department, National Research Center, Dokki 12622, Cairo, Egypt*

[11] *Department of Pharmaceutical Sciences, College of Pharmacy and Thumbay Research Institute for Precision Medicine, Gulf Medical University, Ajman, United Arab Emirates.*

[12] *Department of Pharmaceutical Organic Chemistry, Faculty of Pharmacy, Cairo University, Cairo, Egypt.*

*Corresponding author: W. M. Eldehna wagdy2000@gmail.com, H. O. Tawfik haytham.omar.mahmoud@pharm.tanta.edu.eg.

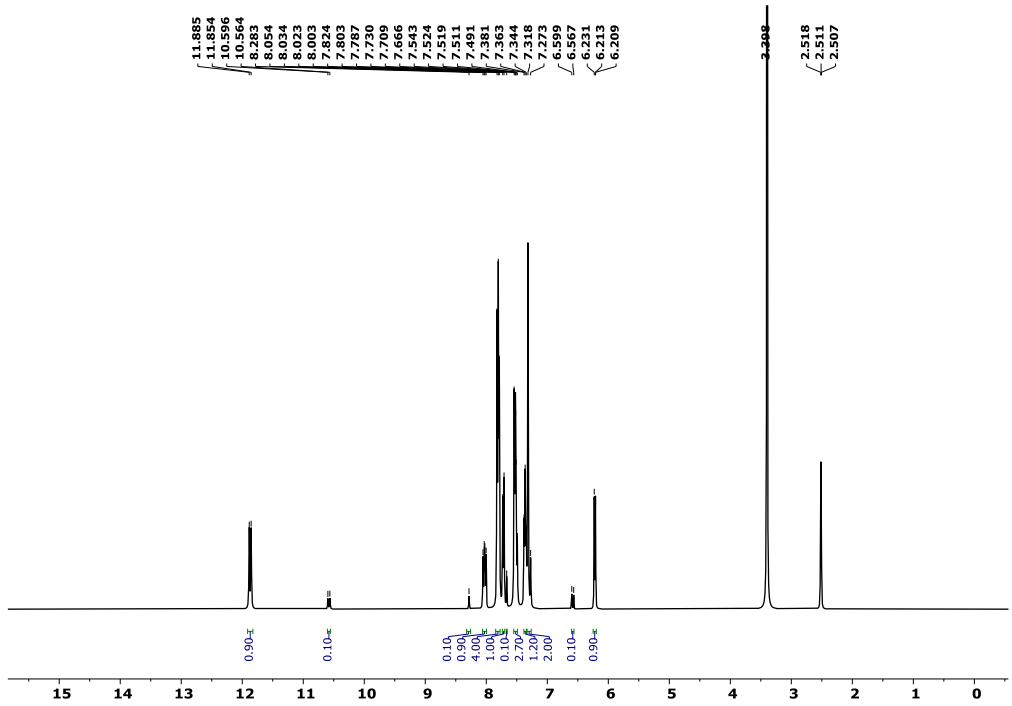


**Figure S1.** $^{1}$H NMR (400 MHz, DMSO$d_6$) spectrum of compound **4a**

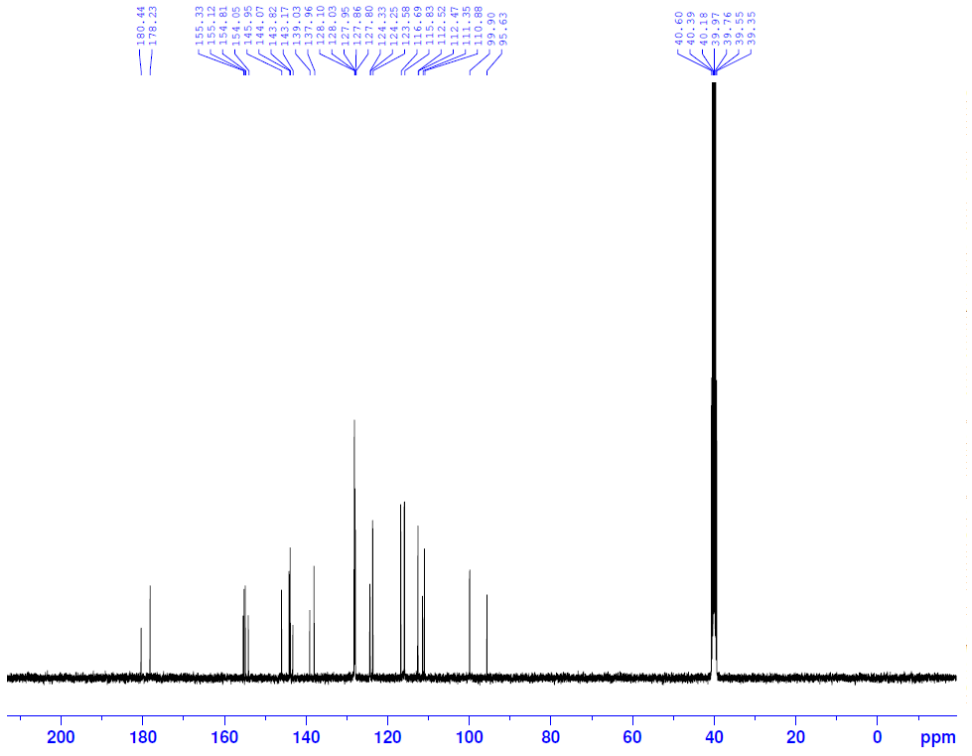


**Figure S2.** $^{13}$C NMR (101 MHz, DMSO$d_6$) spectrum of compound **4a**

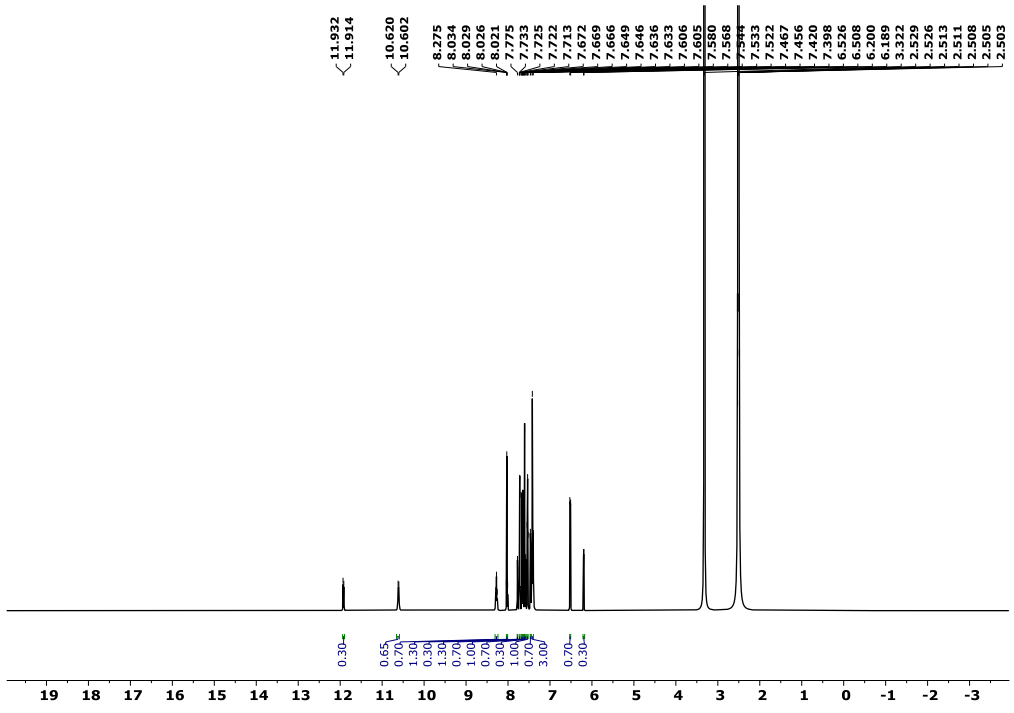

**Figure S3.** $^{1}$H NMR (700 MHz, DMSO$d_6$) spectrum of compound **4b**

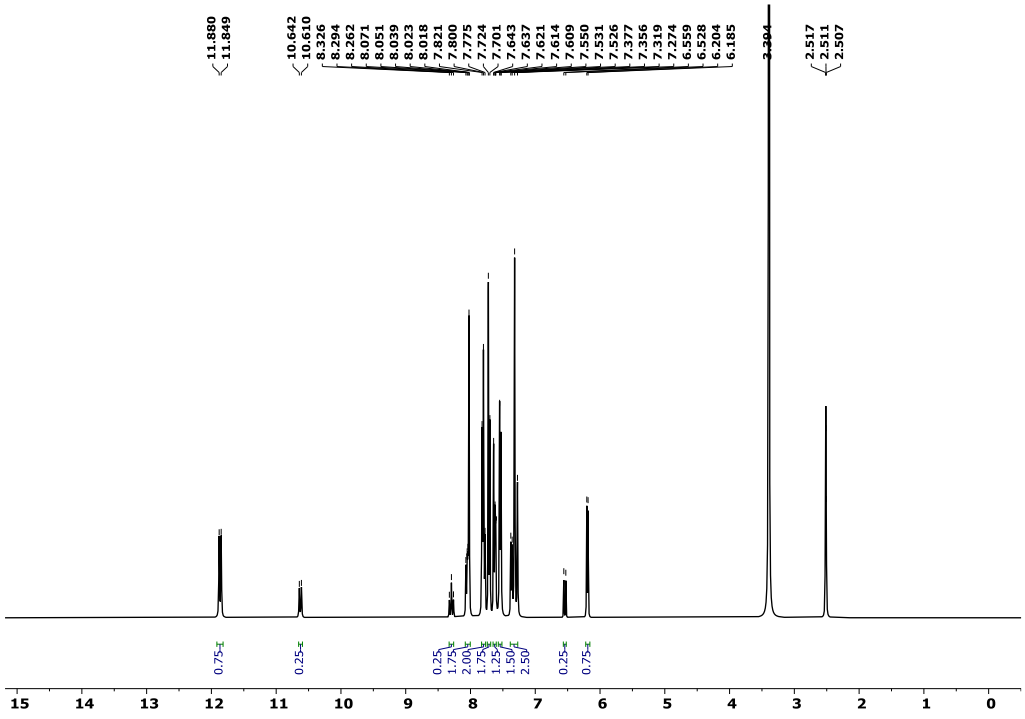

**Figure S4.** $^{1}$H NMR (400 MHz, DMSO$d_6$) spectrum of compound **4c**

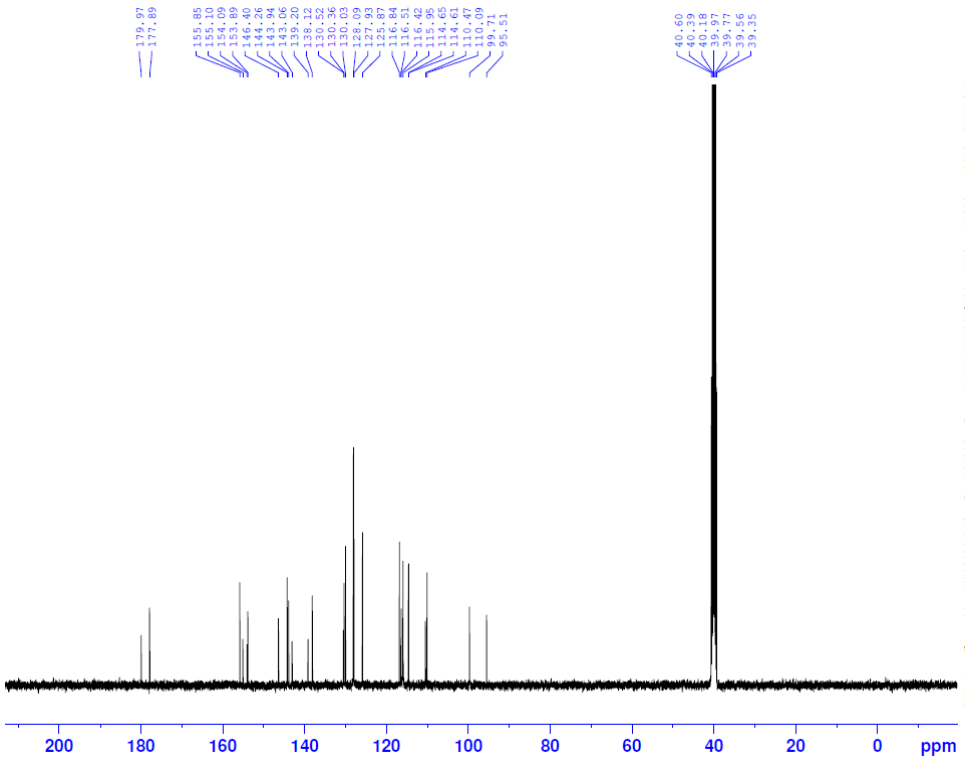


**Figure S5.** $^{13}$C NMR (101 MHz, DMSO$d_6$) spectrum of compound **4c**

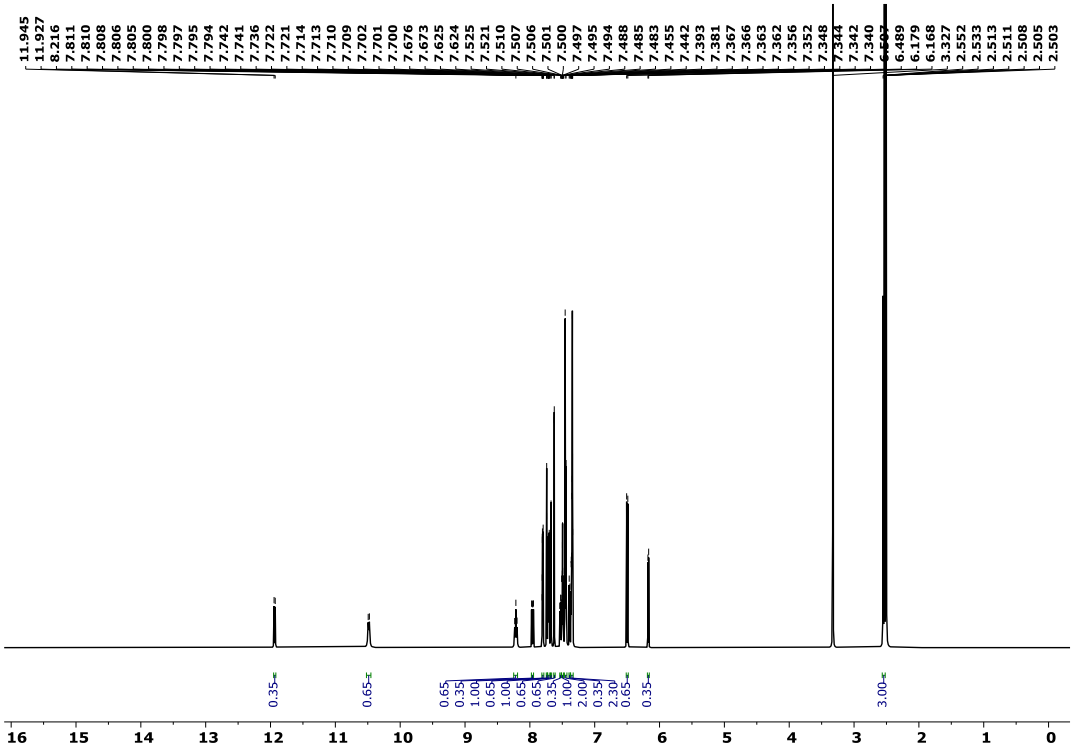


**Figure S6.** $^{1}$H NMR (700 MHz, DMSO$d_6$) spectrum of compound **6a**

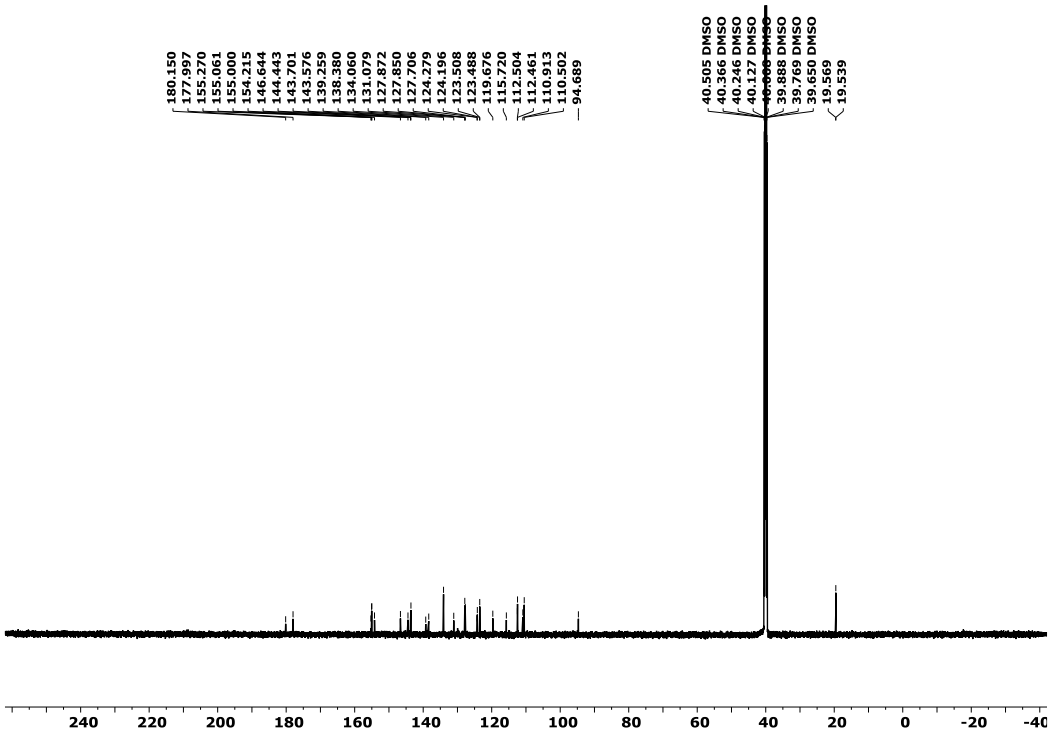


**Figure S7.** $^{13}$C NMR (176 MHz, DMSO$d_6$) spectrum of compound **6a**

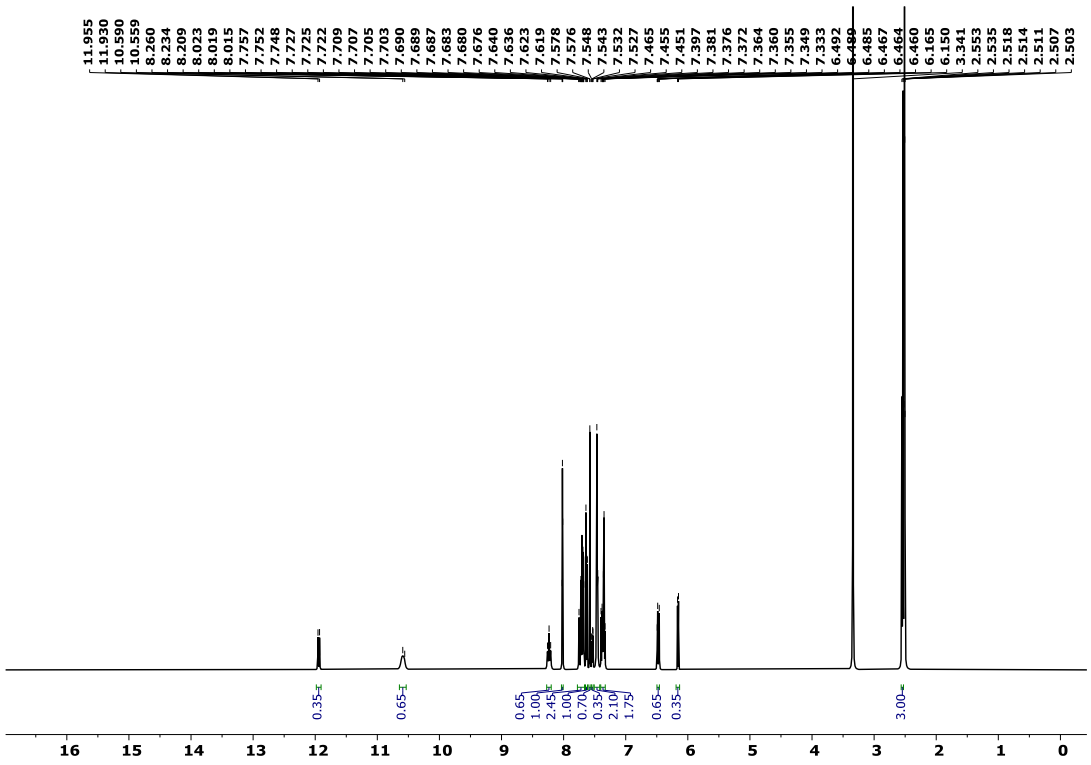


**Figure S8.** $^{1}$H NMR (500 MHz, DMSO$d_6$) spectrum of compound **6b**

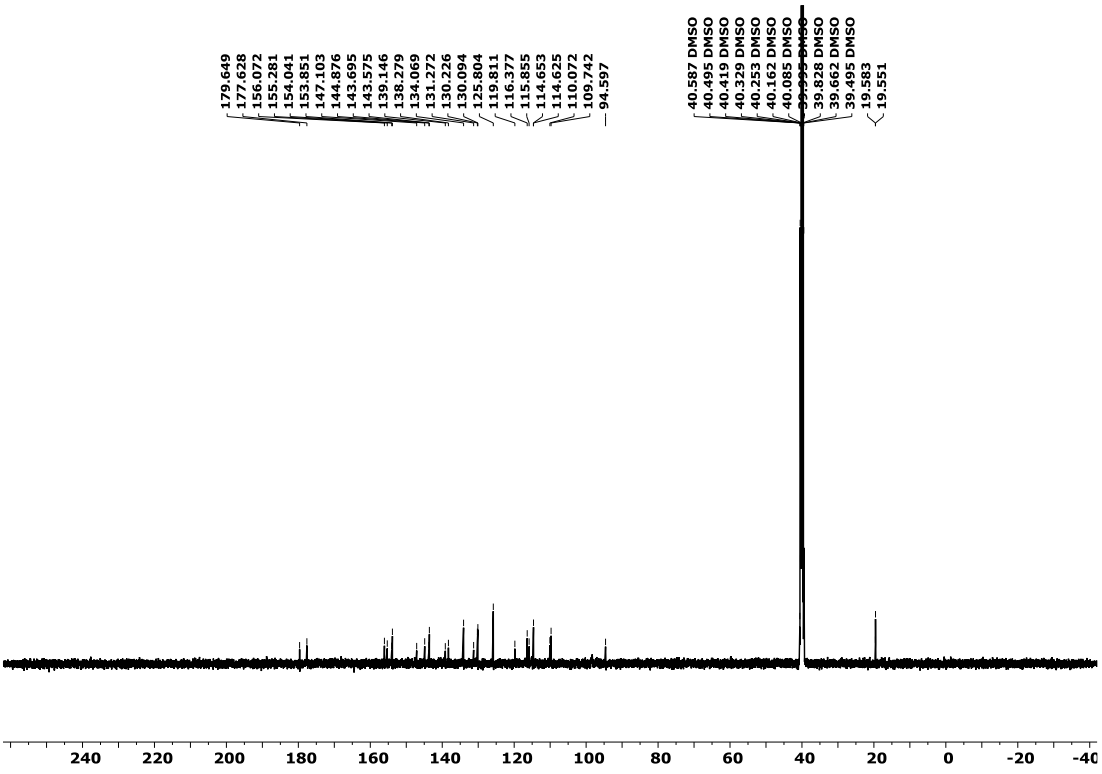


**Figure S9.** $^{13}$C NMR (126 MHz, DMSO$d_6$) spectrum of compound **6b**

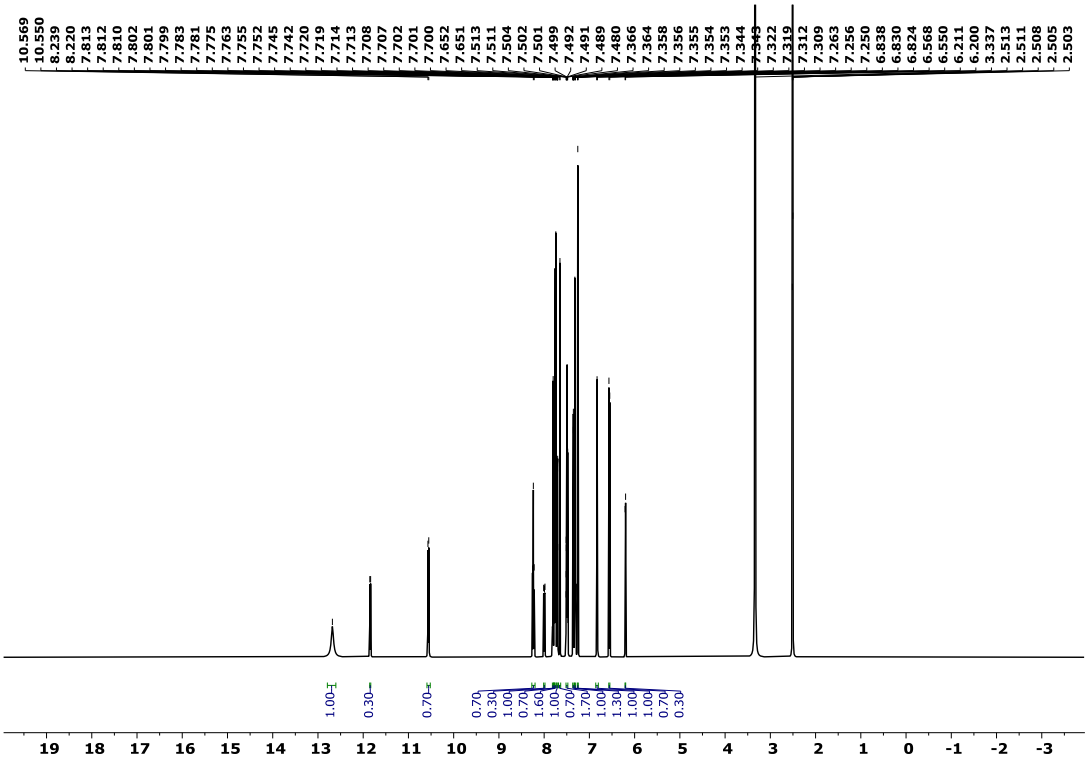


**Figure S10.** $^{1}$H NMR (700 MHz, DMSO$d_6$) spectrum of compound **8a**

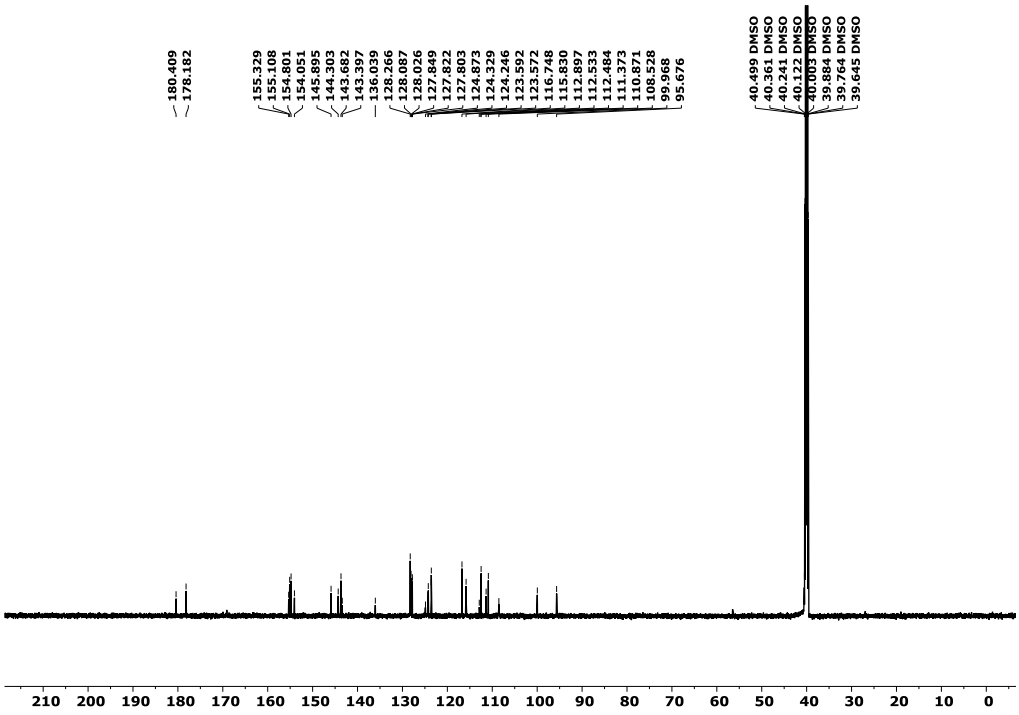


**Figure S11.** $^{13}$C NMR (176 MHz, DMSO$d_6$) spectrum of compound **8a**

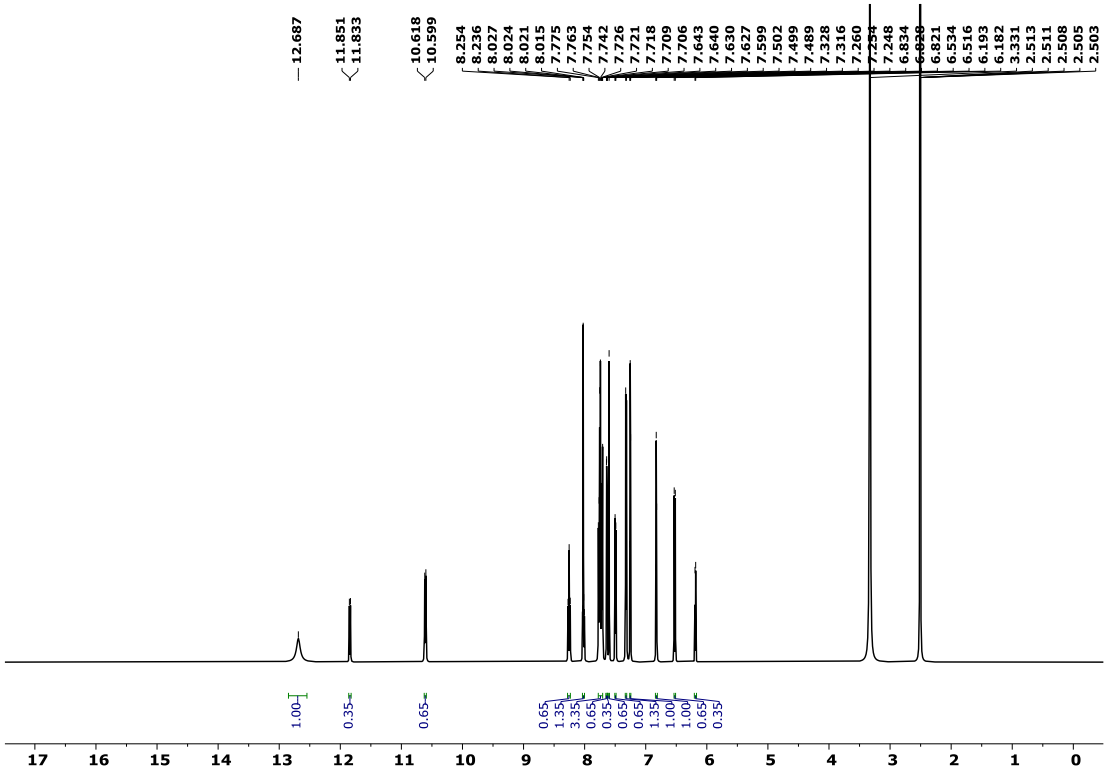


**Figure S12.** $^{1}$H NMR (700 MHz, DMSO$d_6$) spectrum of compound **8b**

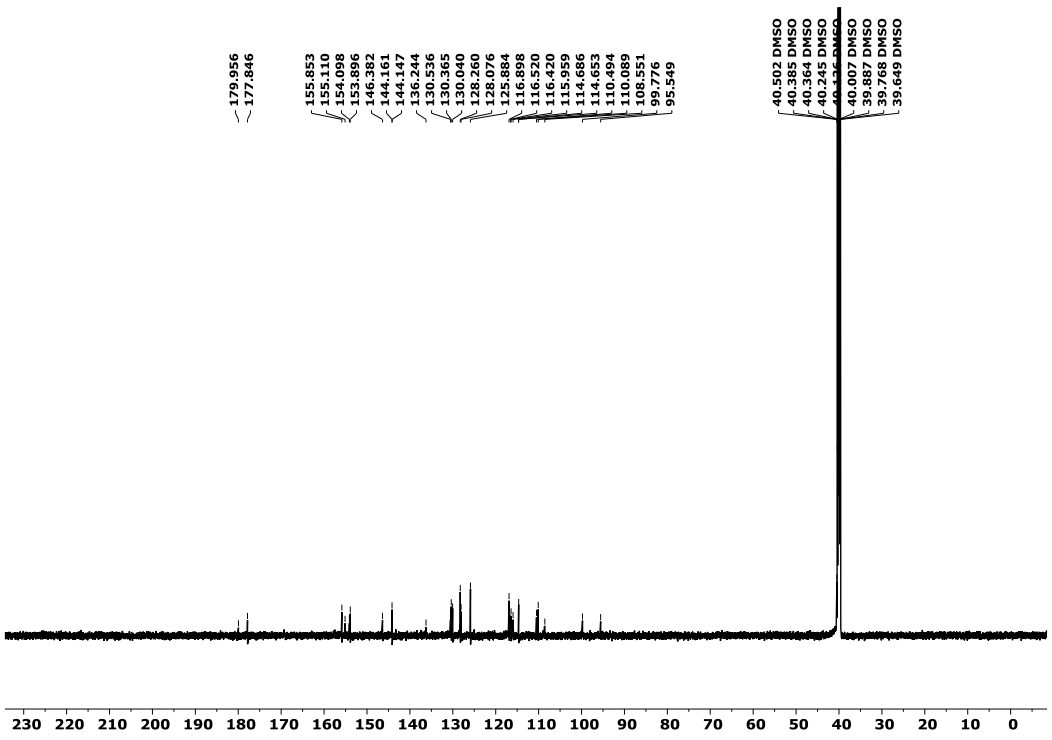


**Figure S13.** $^{13}$C NMR (176 MHz, DMSO$d_6$) spectrum of compound **8b**

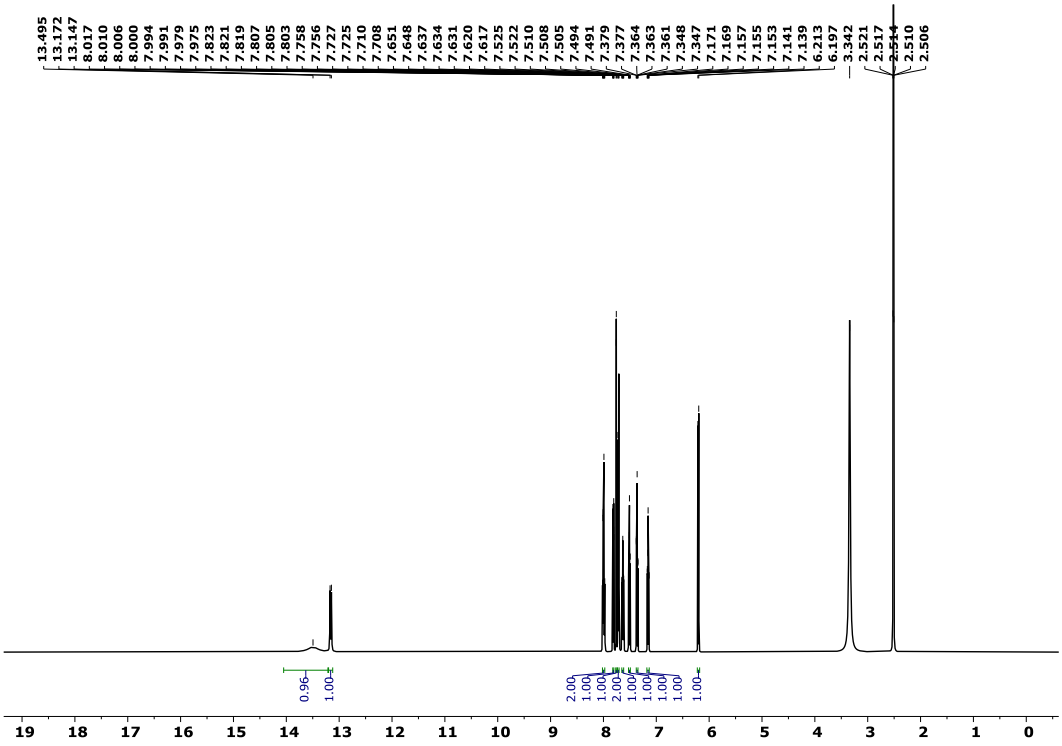


**Figure S14.** $^{1}$H NMR (500 MHz, DMSO$d_6$) spectrum of compound **10a**

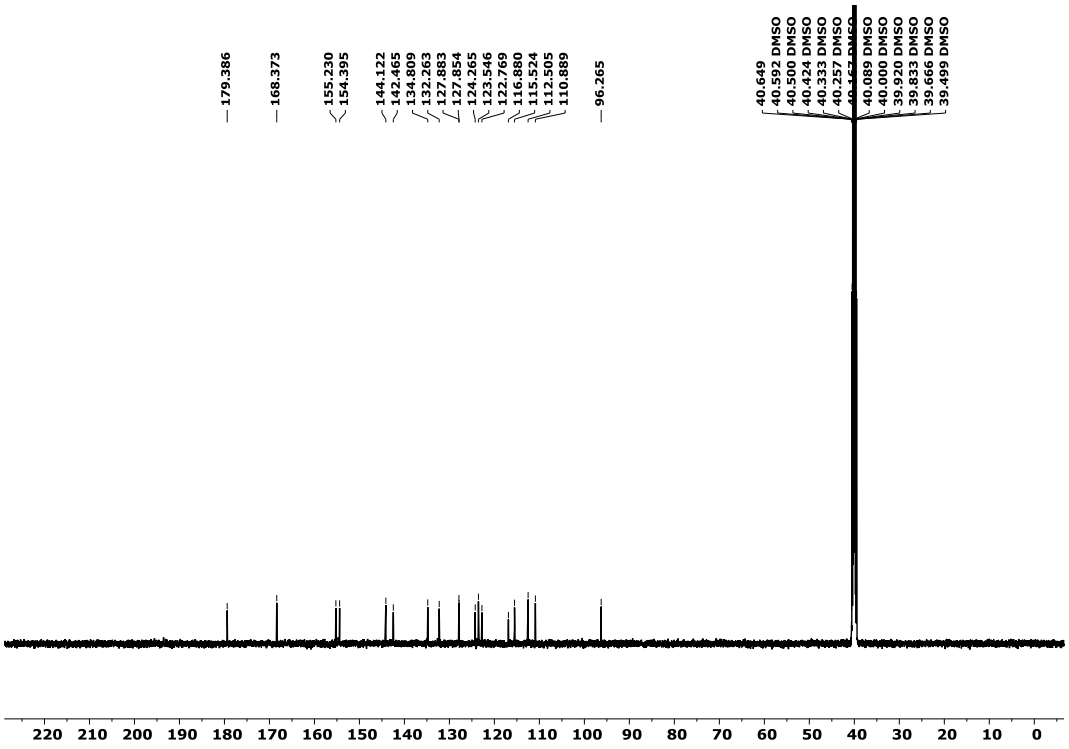


**Figure S15.** $^{13}$C NMR (126 MHz, DMSO$d_6$) spectrum of compound **10a**

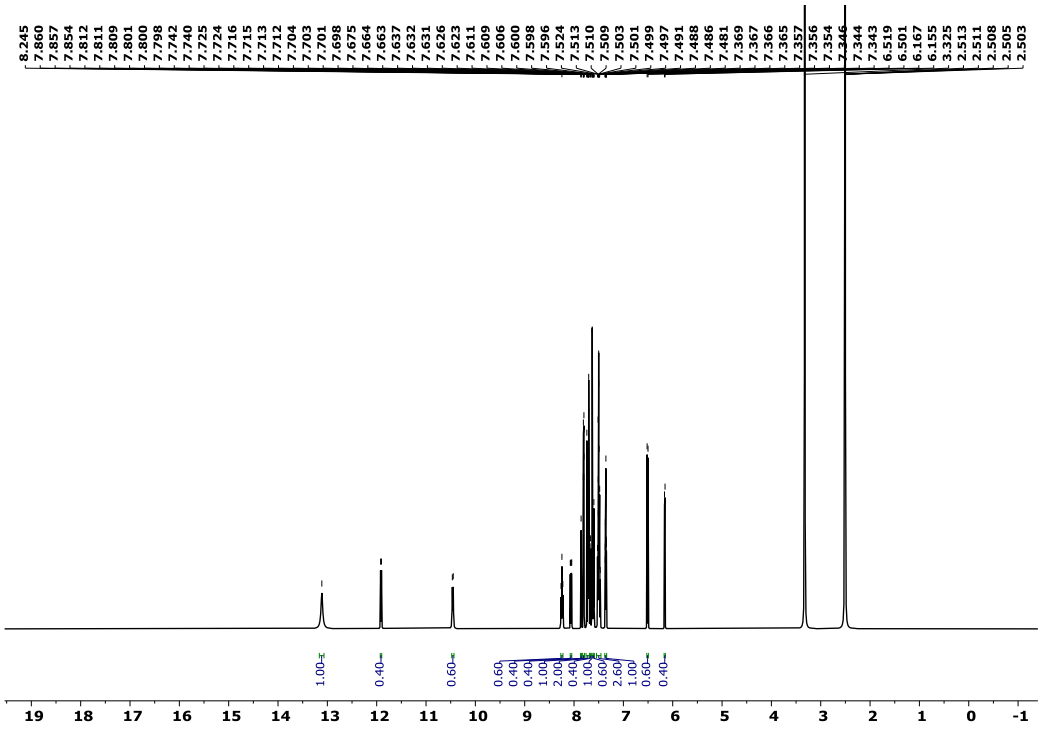


**Figure S16.** $^{1}$H NMR (700 MHz, DMSO$d_6$) spectrum of compound **10b**

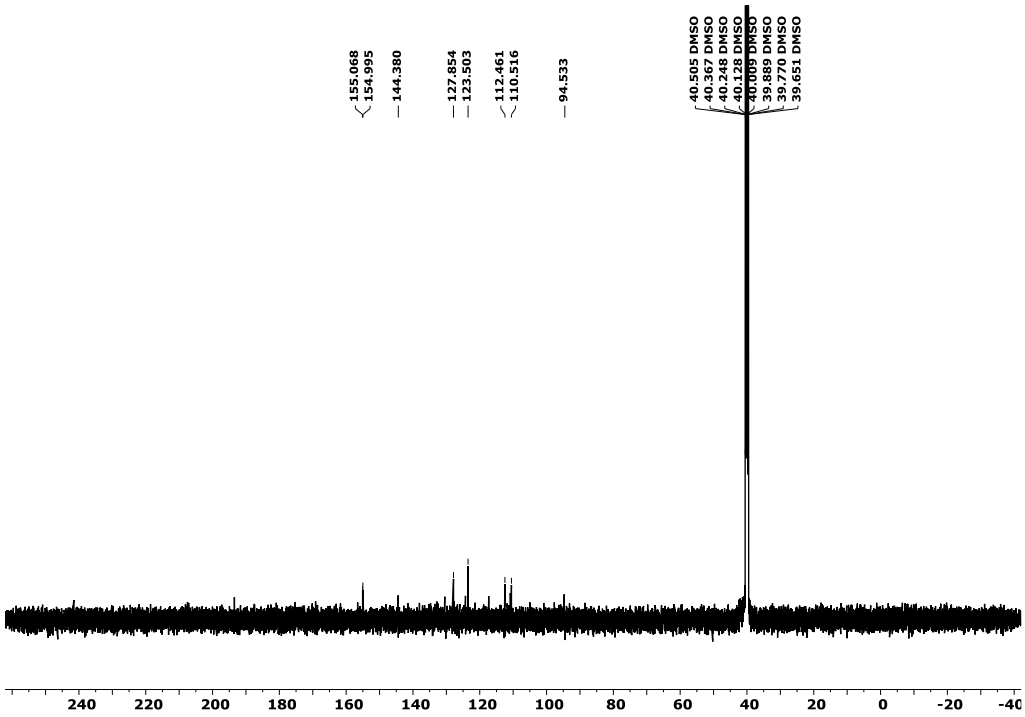


**Figure S17.** $^{13}$C NMR (176 MHz, DMSO$d_6$) spectrum of compound **10b**

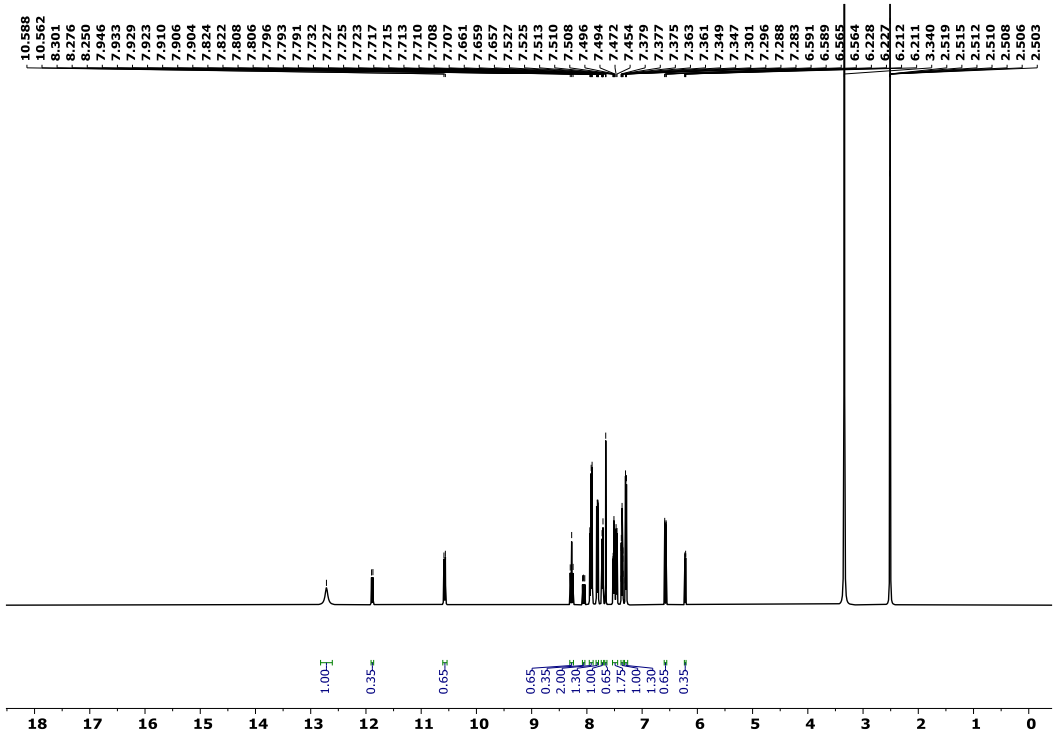


**Figure S18.** $^{1}$H NMR (500 MHz, DMSO$d_6$) spectrum of compound **10c**

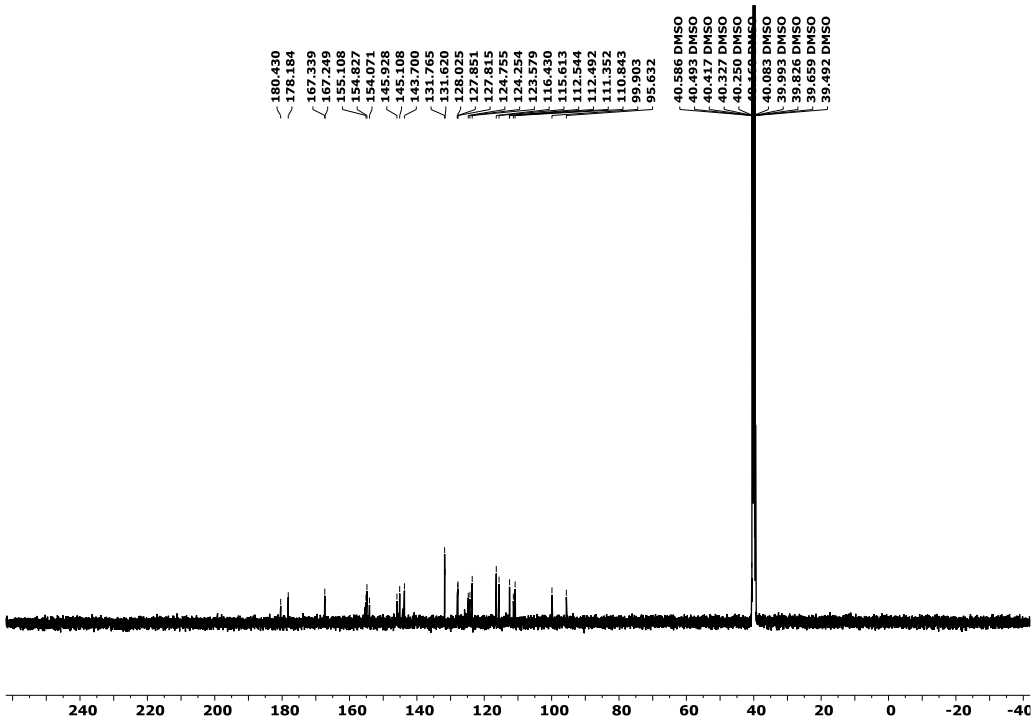


**Figure S19.** $^{13}$C NMR (126 MHz, DMSO$d_6$) spectrum of compound **10c**

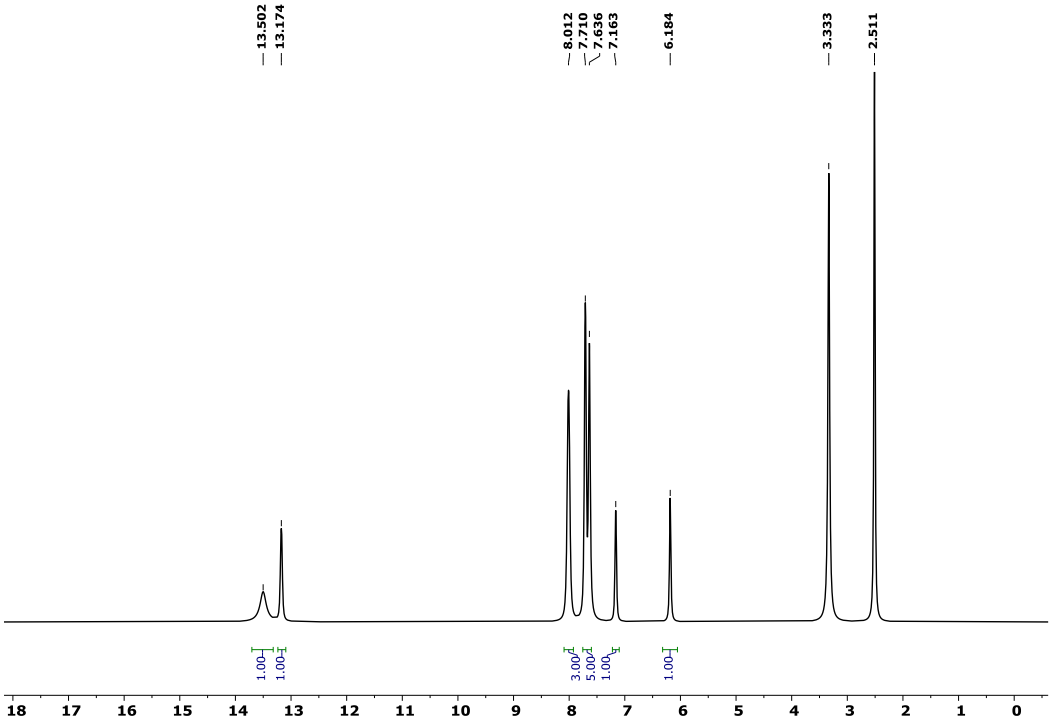


**Figure S20.** $^{1}$H NMR (700 MHz, DMSO$d_6$) spectrum of compound **10d**

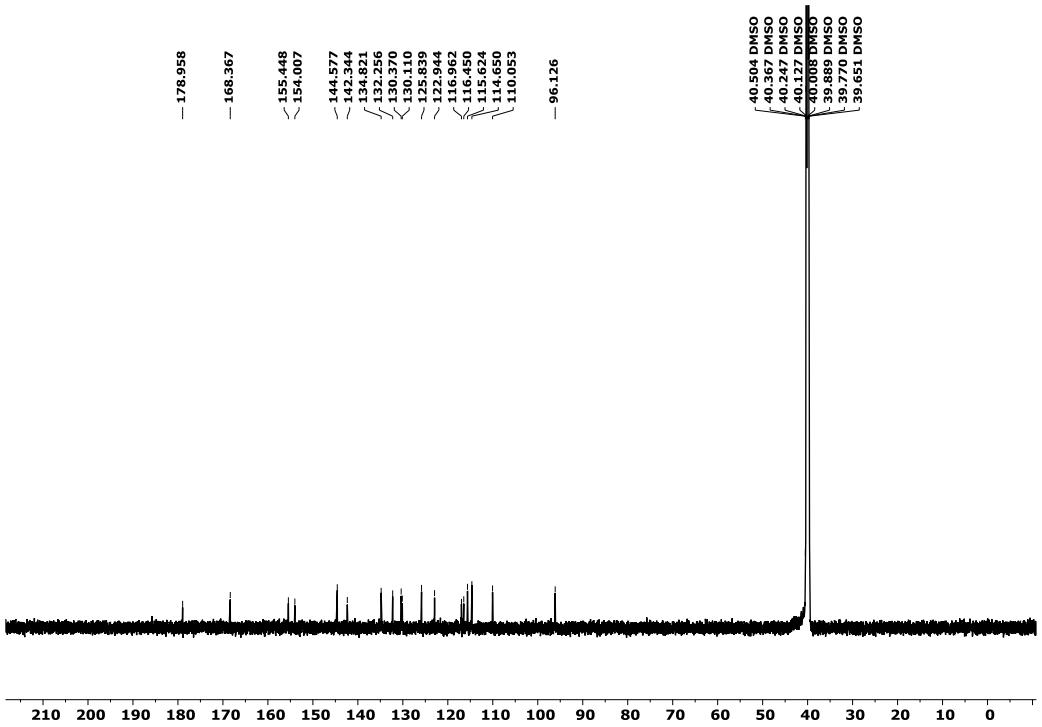


**Figure S21.** $^{13}$C NMR (176 MHz, DMSO$d_6$) spectrum of compound **10d**

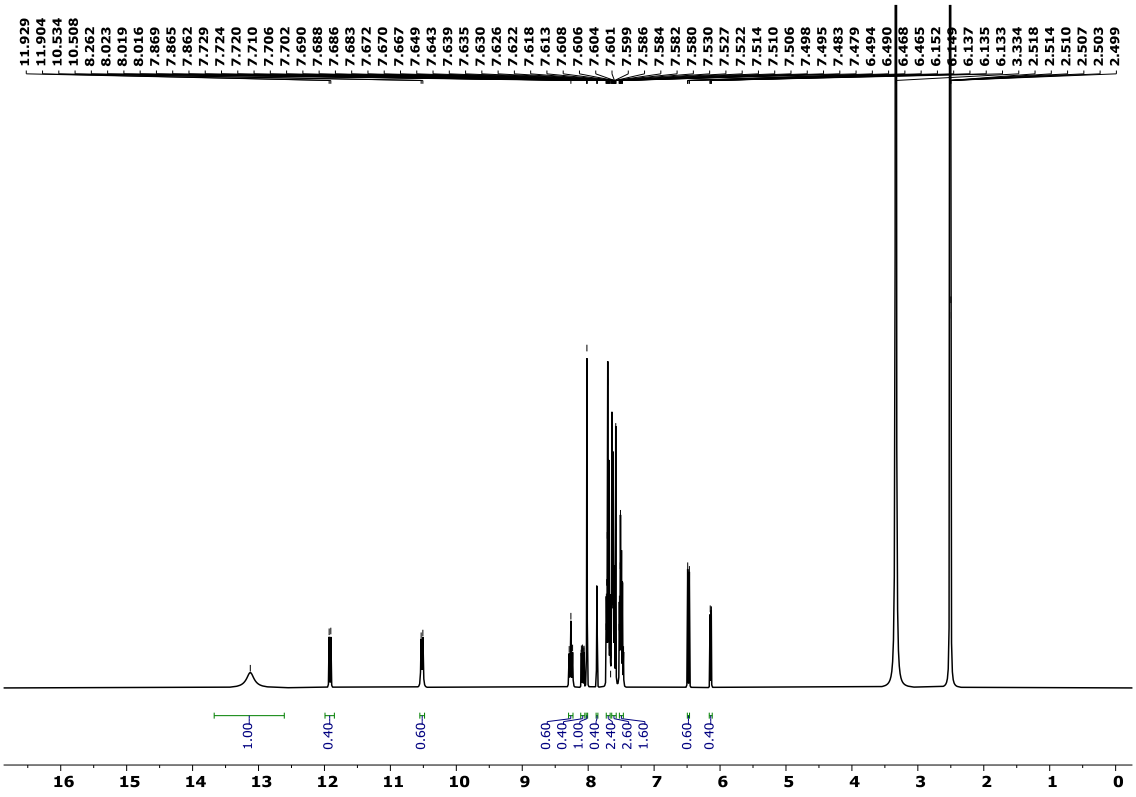


**Figure S22.** $^{1}$H NMR (500 MHz, DMSO$d_6$) spectrum of compound **10e**

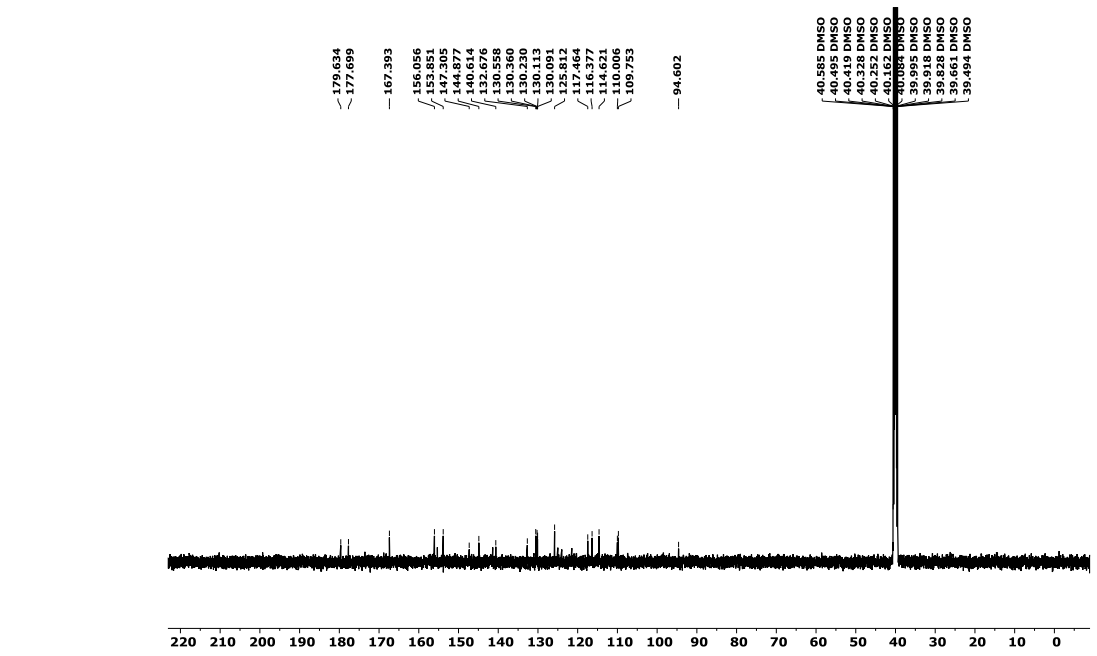


**Figure S23.** $^{13}$C NMR (126 MHz, DMSO$d_6$) spectrum of compound **10e**

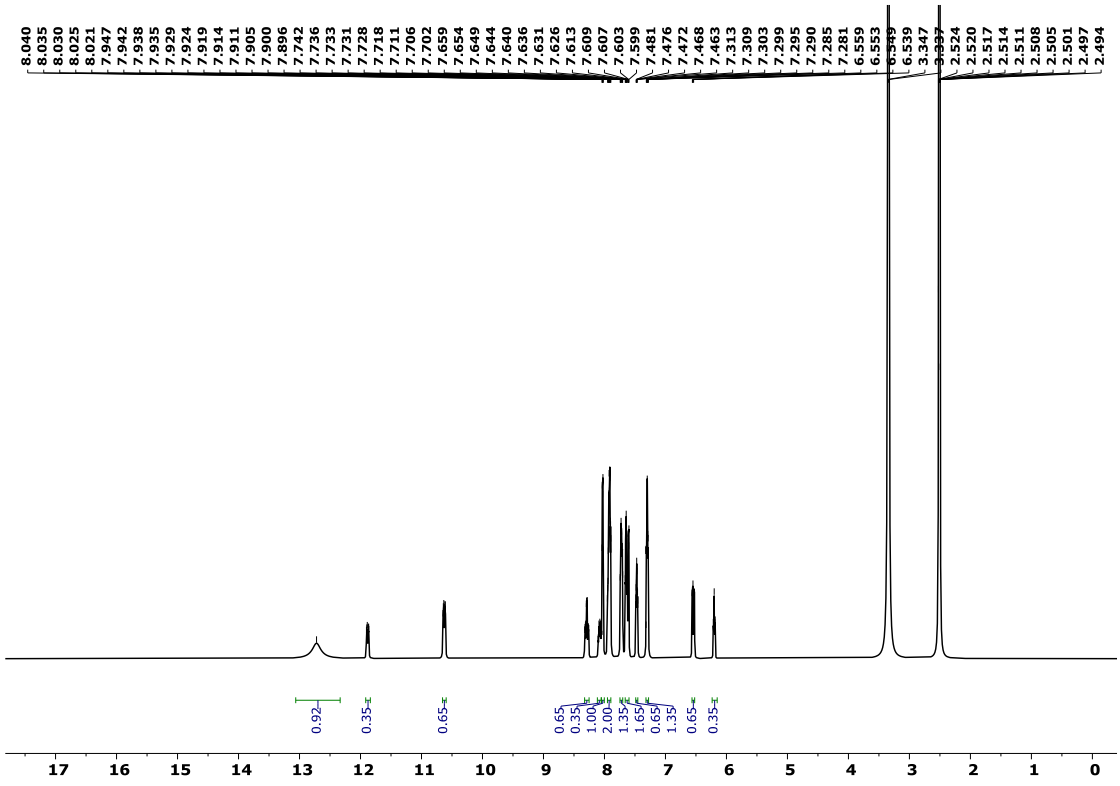


**Figure S24.** $^{1}$H NMR (500 MHz, DMSO$d_6$) spectrum of compound **10f**

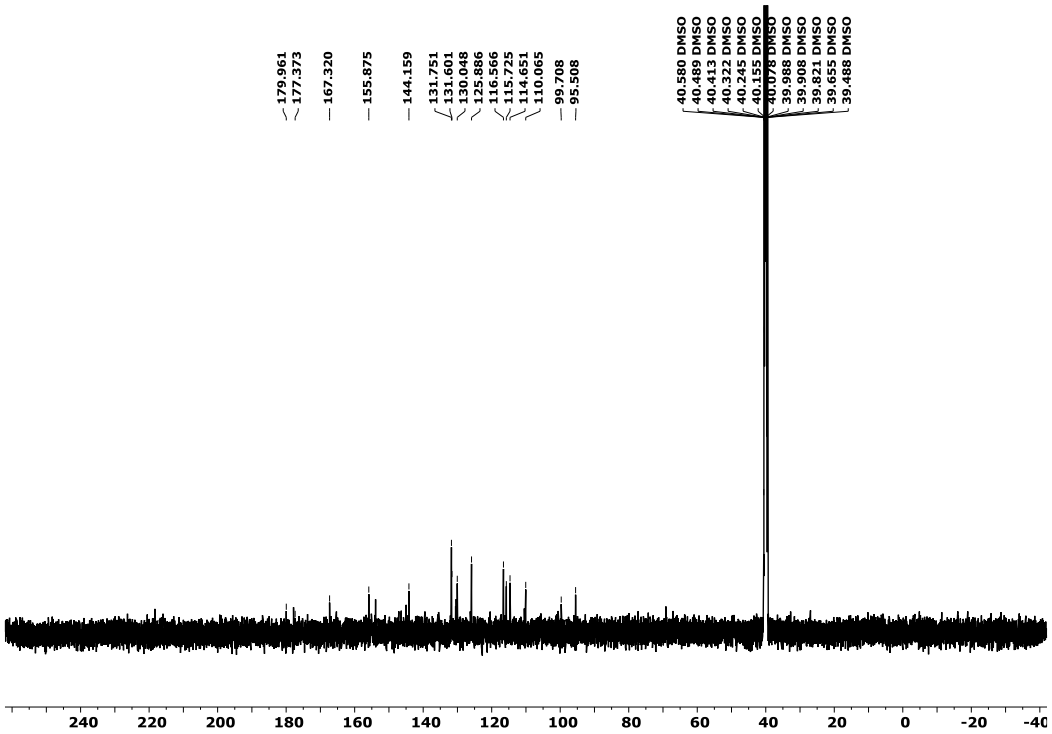


**Figure S25.** $^{13}$C NMR (126 MHz, DMSO$d_6$) spectrum of compound **10f**

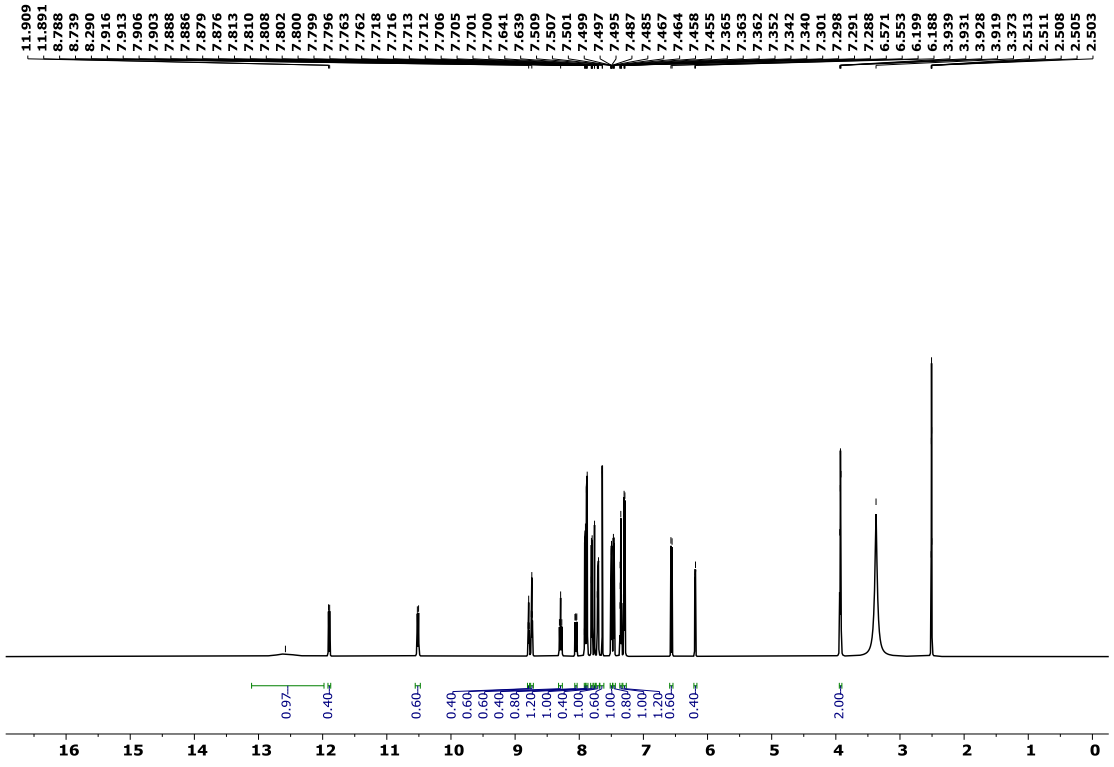


**Figure S26.** $^{1}$H NMR (700 MHz, DMSO$d_6$) spectrum of compound **12a**

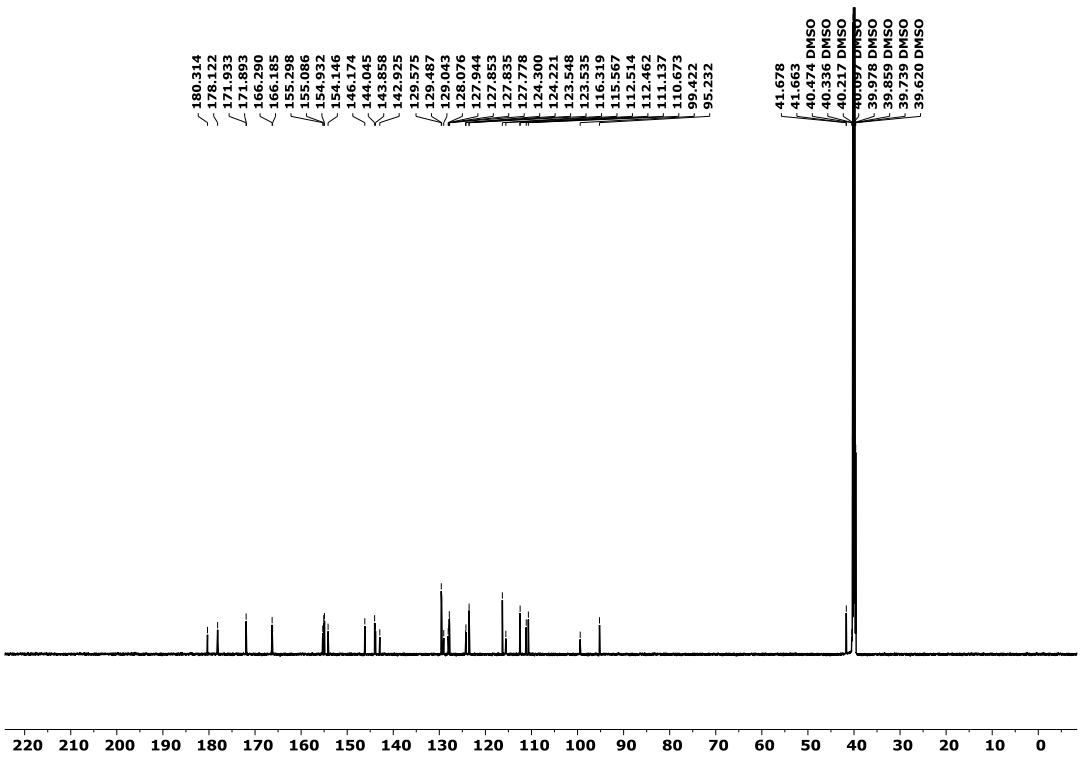


**Figure S27.** $^{13}$C NMR (176 MHz, DMSO$d_6$) spectrum of compound **12a**

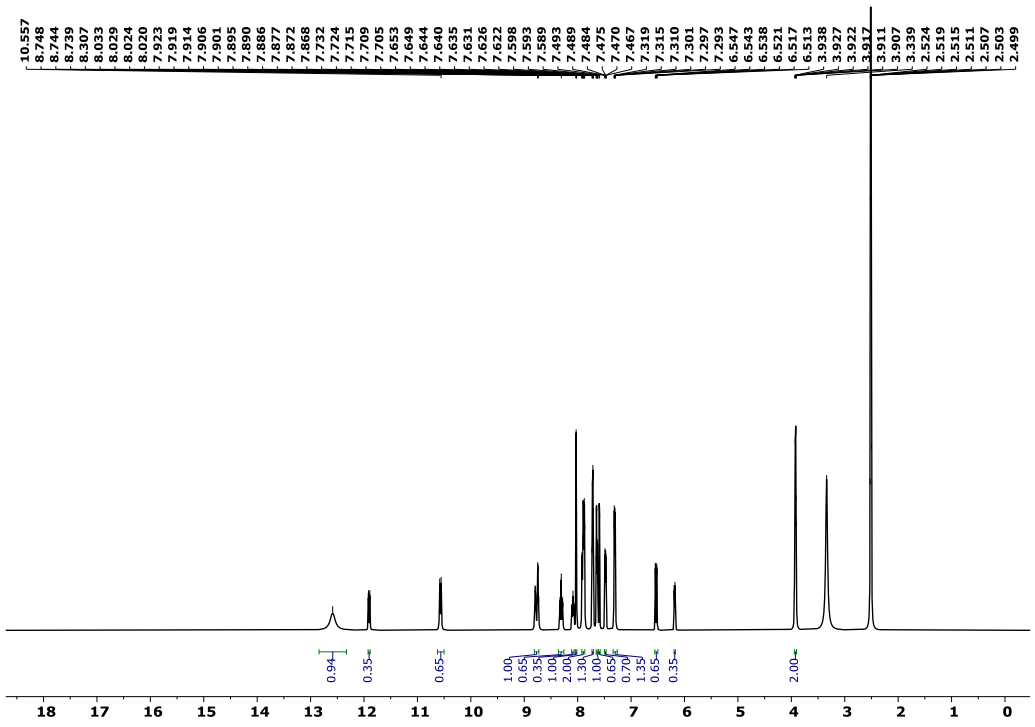


**Figure S28.** $^{1}$H NMR (500 MHz, DMSO$d_6$) spectrum of compound **12b**

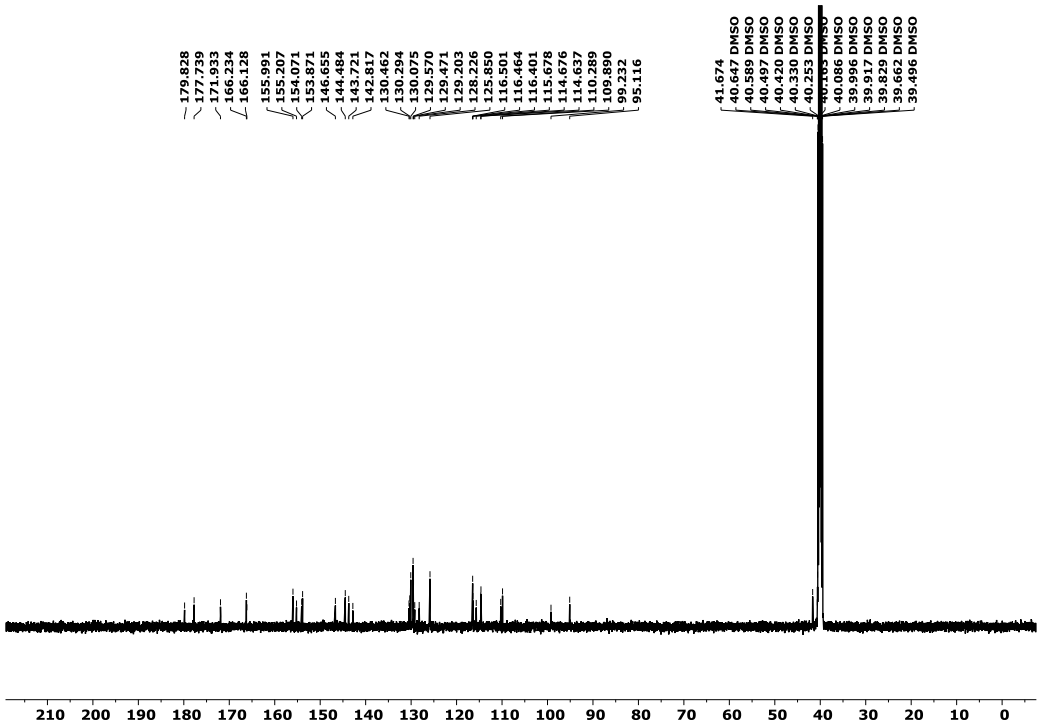


**Figure S29.** $^{13}$C NMR (126 MHz, DMSO$d_6$) spectrum of compound **12b**

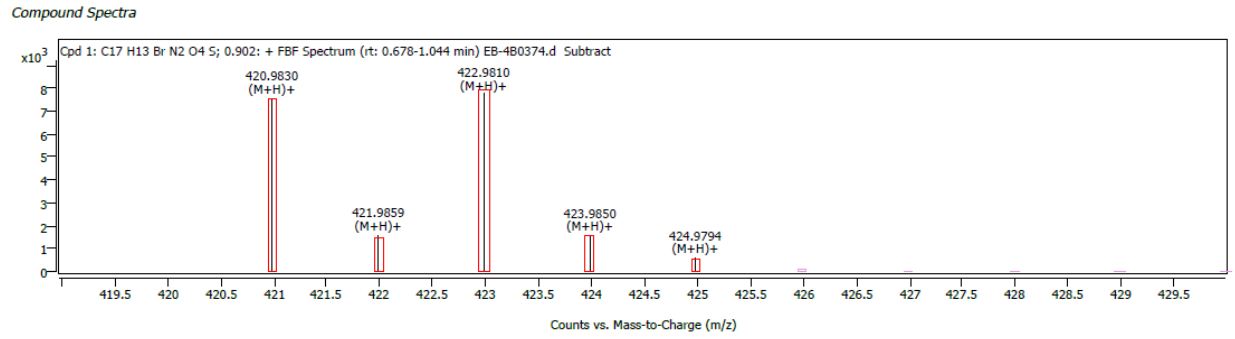


**Figure S30.** HRMS spectrum of compound **4b**

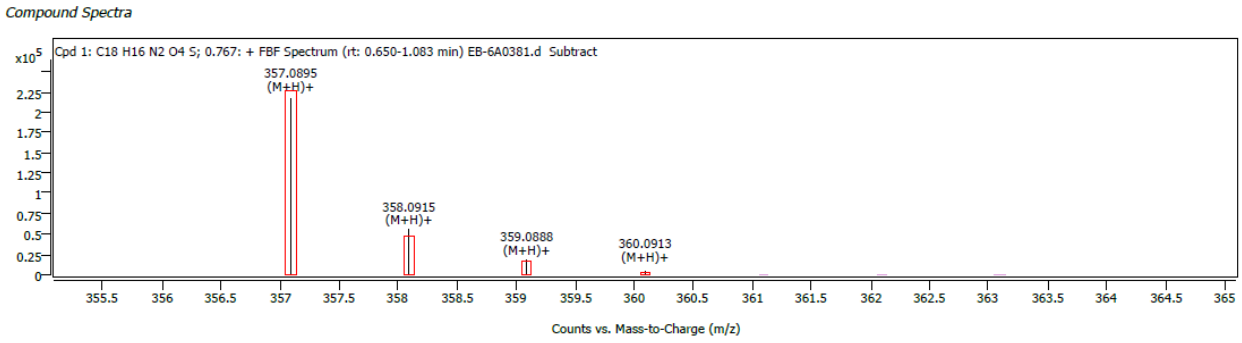


**Figure S31.** HRMS spectrum of compound **6a**

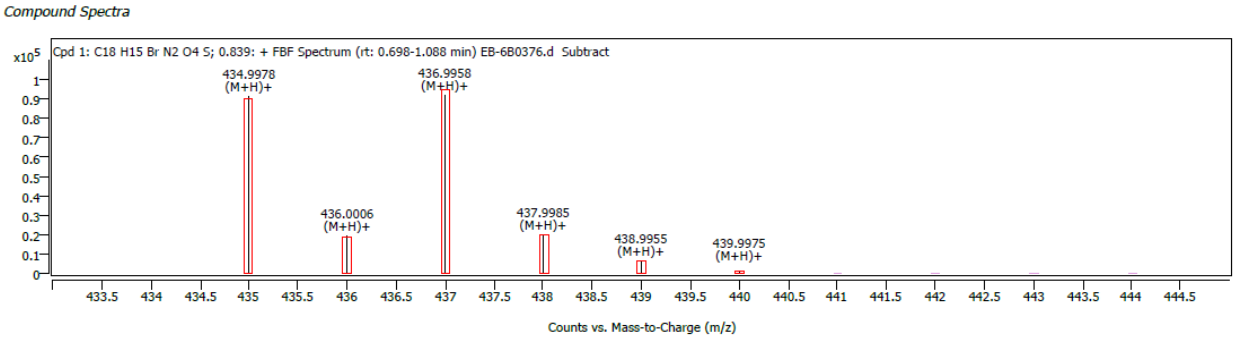


**Figure S32.** HRMS spectrum of compound **6b**

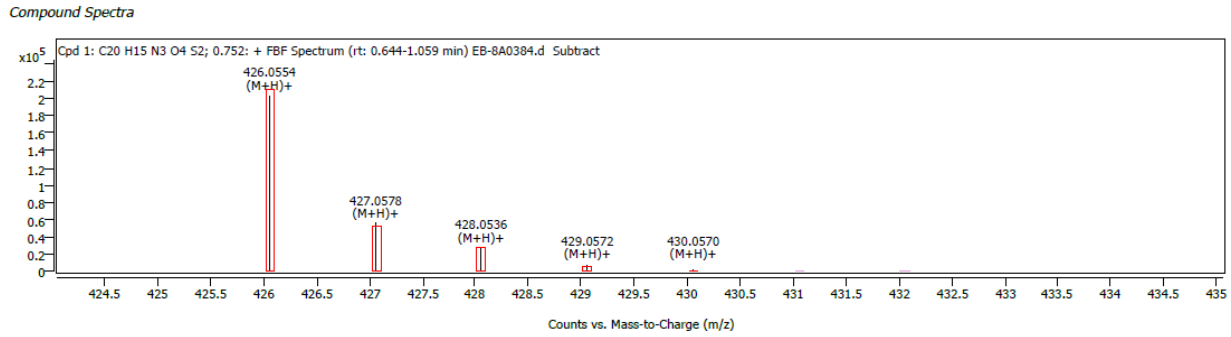


**Figure S33.** HRMS spectrum of compound **8a**

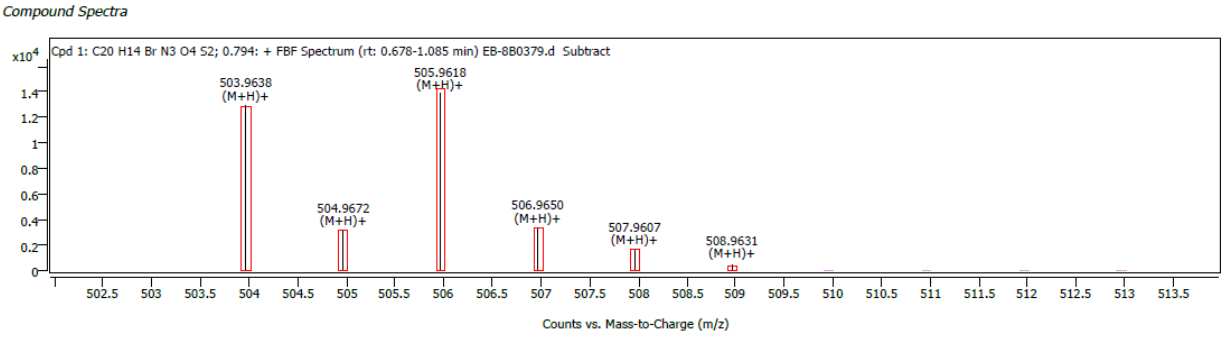


**Figure S34.** HRMS spectrum of compound **8b**

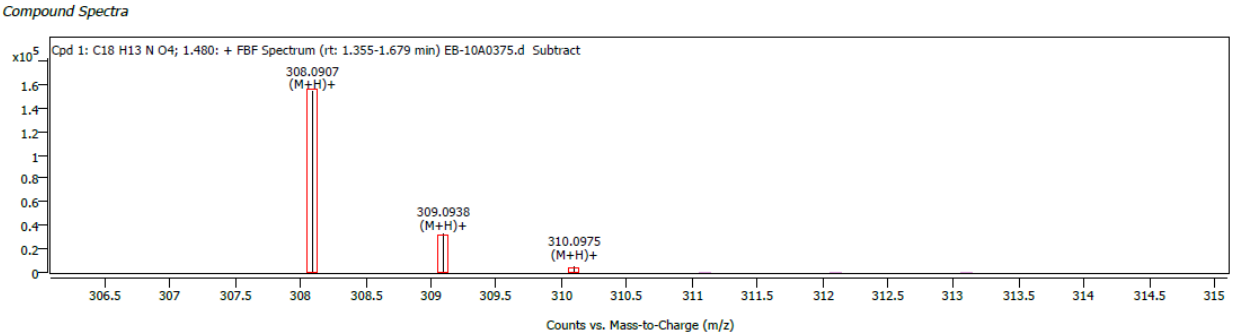


**Figure S35.** HRMS spectrum of compound **10a**

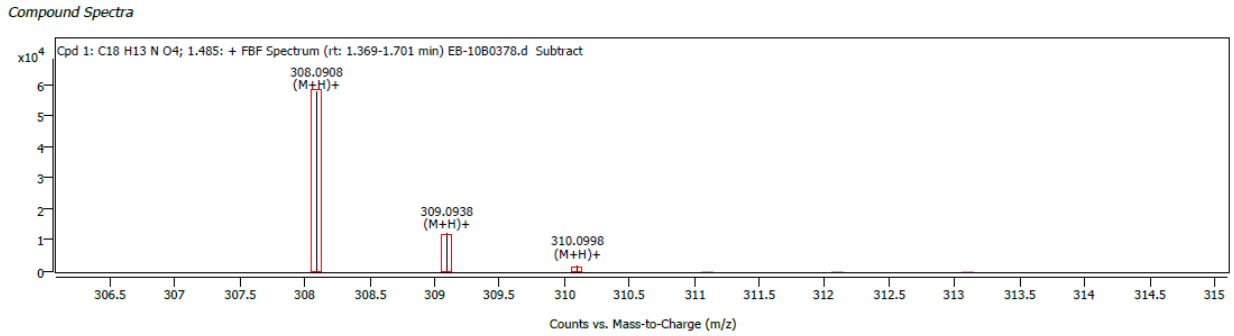


**Figure S36.** HRMS spectrum of compound **10b**

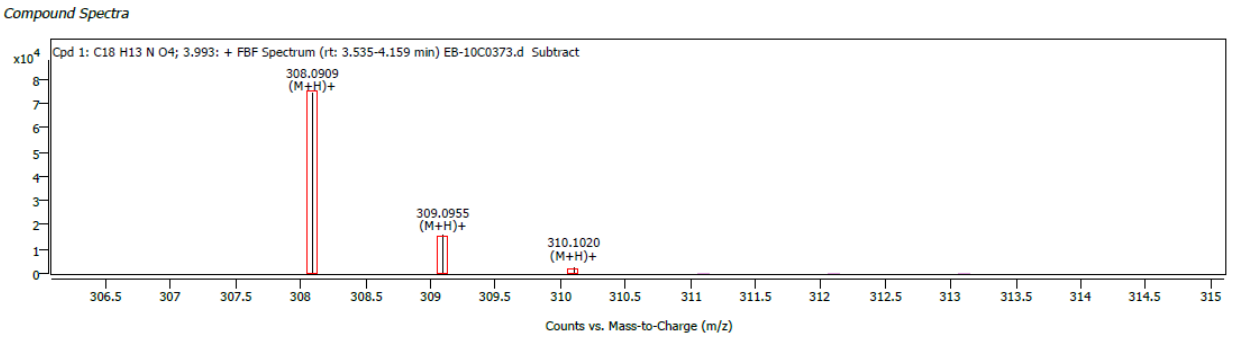


**Figure S37.** HRMS spectrum of compound **10c**

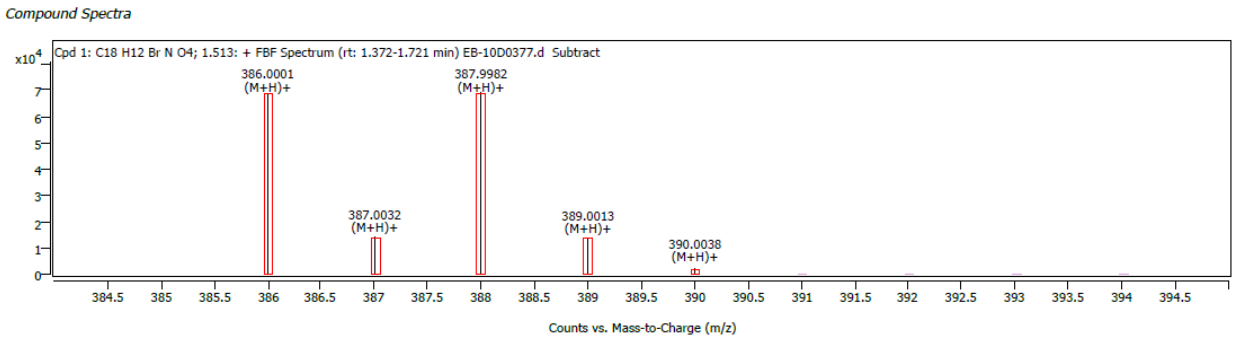


**Figure S38.** HRMS spectrum of compound **10d**

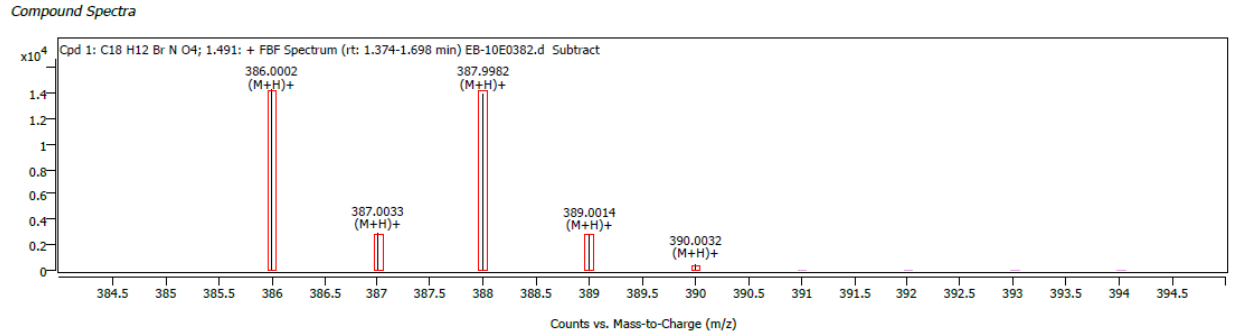


**Figure S39.** HRMS spectrum of compound **10e**

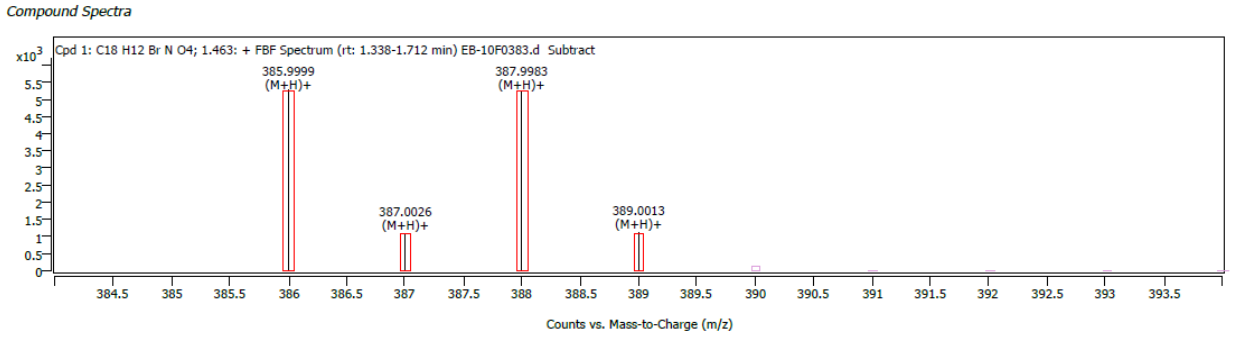


**Figure S40.** HRMS spectrum of compound **10f**

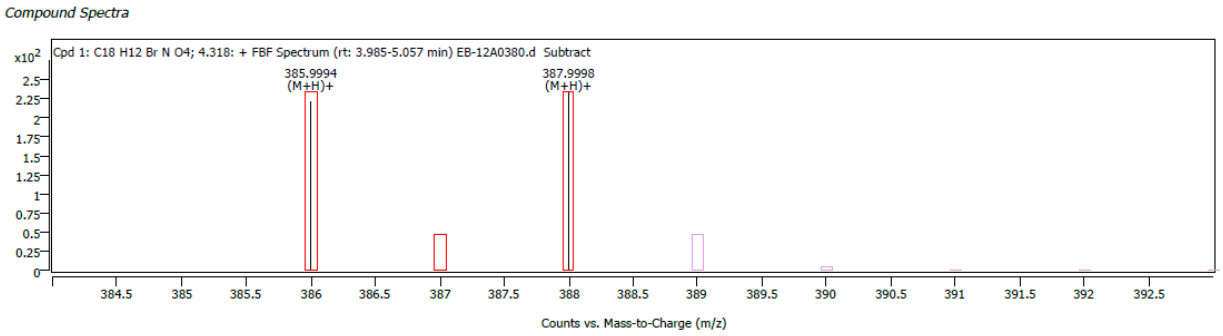


**Figure S41.** HRMS spectrum of compound **12a**

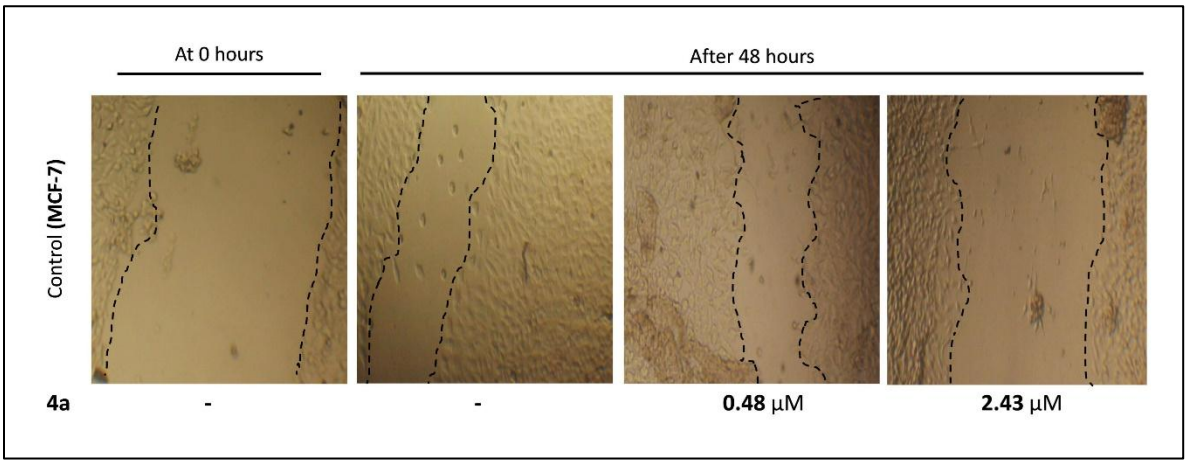


**Figure S42.** Wound-healing assay images illustrating the inhibitory effect of compound **4a** on the migration of MCF-7 cells at 0.1 $IC_{50}$ and 0.5 $IC_{50}$ concentrations compared with the untreated control.

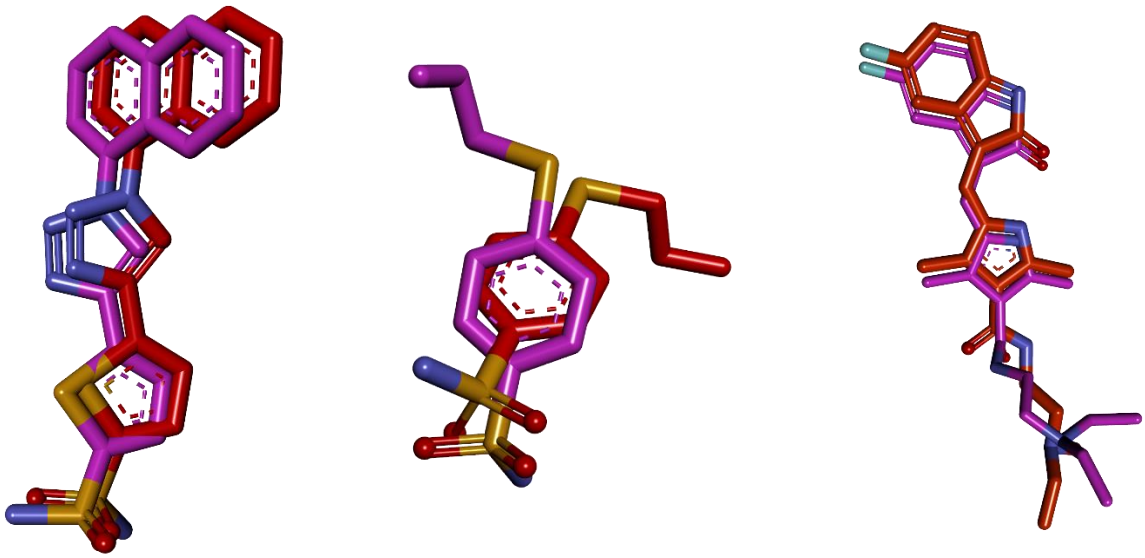

**Figure S43.** Validation of the docking protocol for CA IX (left), CA XII (middle), and VEGFR-2 (right) by redocking the co-crystallized ligands; original ligands shown in orange and redocked poses in pink.

**Biological assessments**

**Human Carbonic Anhydrases (I, IX, and XII) Inhibitory Assay**

The stopped-flow spectrophotometric approach was used to assess the carbonic anhydrase's $CO_2$ hydration activity in the presence of the test substances. The absorbance change of phenol red at 557 nm in HEPES buffer (pH 7.5) was used to measure enzymatic activity. Initial velocities were calculated from several recorded traces after the uncatalyzed reaction rate was adjusted. Prior to measurement, stock solutions of the inhibitors were made in water, diluted with assay buffer, and incubated with the enzyme for fifteen minutes. Nonlinear regression analysis and the Cheng–Prusoff equation were used to determine the kinetic and inhibitory constants ($K_I$). The stated values are the average of a minimum of three separate tests [1-8].

**VEGFR-2 enzyme inhibition**

Commercial assay kits were used to assess the *in vitro* inhibitory activity of the tested compound against the VEGFR-2 kinase (BPS Bioscience, USA). There were eight quantities of the chemical that were serially diluted in DMSO: 3, 1, 0.3, 0.1, 0.03, 0.01, 0.003, and 0.001 μM. A BioTek Synergy2 Microplate Reader (BioTek, USA) was used to measure chemiluminescence and quantify VEGFR-2 kinase activity. The $IC_{50}$ value, which represents the concentration needed to inhibit 50% of kinase activity, was calculated using the dose–response curve (concentration vs. percent residual enzyme activity). Every experiment, including the controls, was conducted three times, and relevant reference standards were used for verification.

***In vitro* anticancer activity**

Dulbecco's Modified Eagle Medium (DMEM) was used to sustain human breast (MCF-7) and prostate (PC-3) cancer cell lines as well as the normal breast MCF-10A cells. It was supplemented with 10% (v/v) fetal bovine serum (FBS), 1% penicillin–streptomycin (100 U/mL and 100 μg/mL, respectively), and insulin (10 μg/mL). The cells were incubated in a humidified environment with 5% $CO_2$ at 37 °C. 100 μM cobalt chloride ($CoCl_2$), which stabilizes HIF-1α and induces a hypoxia-like cellular response, was preloaded onto cells for 72 hours to simulate hypoxic conditions. Before performing the MTT assay, cells were treated with different doses of 5-azacytidine and the produced test compounds for 48 hours following hypoxia induction. Cells were cultivated under normal conditions without the use of $CoCl_2$ for normoxic controls. Following the

incubation time, the MTT colorimetric technique was used to measure cell viability and evaluate the cytotoxic effects of the test substances in both normoxic and hypoxic conditions. Cell lines were obtained from the Holding Company for Biological Products and Vaccines (VACSERA, Giza, Egypt) [9].

**Anticancer adjuvant activity screening**

In MCF-7 and PC-3 cancer cell lines, compound **4a**'s cytotoxic capability was assessed both by itself and in conjunction with doxorubicin (DOX). The cells were incubated at 37 °C in a humidified environment with 5% $CO_2$ in RPMI-1640 media supplemented with 10% heat-inactivated fetal calf serum (FCS) and 50 µg/mL of gentamicin. Cells were pretreated with 100 µM cobalt chloride ($CoCl_2$) for 72 hours before drug exposure in order to create hypoxia. Cells were exposed to DOX, compound **4a**, or both for 48 hours following hypoxia induction. The MTT assay was then used to assess cell viability. In short, each well was filled with MTT solution (5 mg/mL in PBS) and incubated for 4 hours at 37 °C. After dissolving the resultant formazan crystals in DMSO, the absorbance was quantified using a microplate reader at 570 nm. The percentage of viable cells in comparison to untreated controls was used to express the results.

**Cell cycle analysis**

Using a FACSCalibur flow cytometer (BD Biosciences, USA), the impact of compound **4a** on the cell cycle progression of MCF-7 breast cancer cells was examined. In brief, cells were seeded in 6-well plates and treated with compound **4a** for 24 hours under conventional conditions. After treatment, adherent and floating cells were separated, rinsed twice with cold PBS, and then preserved for the entire night at 4 °C in 70% ice-cold ethanol. Following fixation, cells were centrifuged, washed with PBS to eliminate any remaining ethanol, and stained for 30 minutes at room temperature in the dark using a solution containing 50 µg/mL propidium iodide (PI) and 100 µg/mL RNase A in PBS. Following flow cytometry analysis of the samples, CellQuest Pro and ModFit LT software were used to evaluate the data and ascertain the distribution of cells across the $G_0/G_1$, S, and $G_2$/M phases.

**Annexin V-FITC/Propidium Iodide (PI) assay**

Compound **4a**'s ability to induce apoptosis in MCF-7 breast cancer cells was assessed using a flow cytometry (FACSCalibur, BD Biosciences, USA) and an Annexin V-FITC/Propidium Iodide (PI) apoptosis detection kit. In short, compound **4a** was applied for 24 hours after MCF-7 cells were seeded in 6-well plates. Following treatment, adherent and floating cells were separated, rinsed twice with cold PBS, and then resuspended at a density of $1 \times 10^6$ cells/mL in 1× binding buffer. After that, 100 μL of the suspension was mixed with 5 μL of Annexin V-FITC and 5 μL of PI, and the mixture was incubated for 15 minutes at room temperature in the dark. After adding 400 μL of binding buffer, the samples were promptly subjected to flow cytometry analysis. CellQuest Pro software was used to quantify the percentages of necrotic (Annexin $V^-/PI^+$), early apoptotic (Annexin $V^+/PI^-$), late apoptotic (Annexin $V^+/PI^+$), and viable (Annexin $V^-/PI^-$) cells.

**The cell migration of MCF-7 cells**

The ability of MCF-7 cells to migrate in the presence of resveratrol and its analogues was assessed using a wound healing test. MCF-7 cells were planted in a 12-well plate at a density of $1.5 \times 10^6$ cells per well. A 200 μL pipette tip was used to make a scratch across the cell monolayer following a 24-hour incubation period. The remaining cells were treated with 3 μM resveratrol or its analogues after detached cells were eliminated by washing with fresh media. ImageJ software was used to quantify the wound area after photos of the wound were taken at 0 and 48 hours. Three replicates were used for each experiment in the triplicate migration assay.

**Physicochemical factors and pharmacokinetic properties *in silico* forecasts**

Using the ADMETlab 3.0 online platform, which combines several predictive models for a thorough evaluation of drug-likeness and ADMET (Absorption, Distribution, Metabolism, Excretion, and Toxicity) parameters, the physicochemical, pharmacokinetic, and toxicity-related properties of the synthesized compounds were predicted. Key physicochemical parameters, including molecular weight (MW), topological polar surface area (TPSA), lipophilicity (LogP), hydrogen bond donors (HBD), and acceptors (HBA), were estimated as part of the investigation, along with adherence to Lipinski's and Veber's principles. Human intestinal absorption (HIA), Caco-2 permeability, blood-brain barrier (BBB) penetration, and plasma protein binding (PPB)

were all included in the pharmacokinetic projections. Prior to experimental validation, these thorough *in silico* assessments offered insightful information on the safety profiles and drug-likeness of the studied compounds [10, 11].

**Docking Protocol**

Receptor and ligand preparation and docking were performed to investigate the binding interactions of compound **4a** against human carbonic anhydrase IX (PDB ID: 5FL4), carbonic anhydrase XII (PDB ID: 4WW8), and VEGFR-2 (PDB ID: 4AGD). For each target, crystal structures were cleaned by removing crystallographic waters and co-crystallized ligands; the catalytic Zn(II) ion was retained only for CA IX and CA XII. Missing residues were modelled and fixed using MODELLER 10.4; afterwards, all missing heavy atoms and protonation states were checked. Polar hydrogens were added, and atom types/partial charges were assigned according to the AD4Zn parameter set for CA IX and CA XII, while VEGFR-2 atom types/charges were assigned using the standard AutoDock parameterization; receptors were then exported as PDBQT files. Compound **4a** was prepared by adding hydrogens, assigning Gasteiger-type partial charges, defining rotatable bonds, and saving it as a PDBQT file. Grid boxes were defined as follows: CA IX (5FL4) — spacing 0.375 Å, npts 50 × 40 × 40, center = 14.269, -27.594, 60.641 (box dimensions = 18.75 × 15.00 × 15.00 Å); CA XII (4WW8) — spacing 0.375 Å, npts 40 × 58 × 40, center = 25.793, 3.267, 10.512 (box dimensions = 15.00 × 21.75 × 15.00 Å); VEGFR-2 (4AGD) — spacing 1.0 Å, npts 22 × 22 × 22, center = 50.579, -1.304, -11.753 (box dimensions = 22 × 22 × 22 Å). Docking runs were executed with AutoDock Vina v1.2.3, using the AD4Zn scoring/parameterization for CA IX and CA XII and standard Vina parameterization for VEGFR-2, with search parameters set to exhaustiveness = 32, num_modes = 9, and energy_range = 3 kcal/mol unless otherwise stated. The resulting poses were ranked by predicted affinity and visually inspected in Discovery Studio Visualizer v21.1.0.20298 to verify the correct Zn coordination geometry, hydrogen bonds, hydrophobic/π interactions, and other key active-site contacts. Representative top poses of **4a** were saved for further analysis and figure generation.

**References**


[1] S.M. Hefny, T.F. El-Moselhy, N. El-Din, A. Ammara, A. Angeli, M. Ferraroni, A.M. El-Dessouki, M.A. Shaldam, G. Yahya, A.A. Al-Karmalawy, C.T. Supuran, H.O. Tawfik, A new framework for novel analogues of pazopanib as potent and selective human carbonic anhydrase inhibitors: Design, repurposing rational, synthesis, crystallographic, in vivo and in vitro biological assessments, European Journal of Medicinal Chemistry, 274 (2024) 1-19.

[2] S.M. Hefny, T.F. El-Moselhy, N. El-Din, S. Giovannuzzi, T. Bin Traiki, M.-A. Vaali-Mohammed, A.M. El-Dessouki, K. Yamaguchi, M. Sugiura, M.A. Shaldam, C.T. Supuran, M.-H. Abdulla, W.M. Eldehna, H.O. Tawfik, Discovery and mechanistic studies of dual-target hits for carbonic anhydrase IX and VEGFR-2 as potential agents for solid tumors: X-ray, in vitro, in vivo, and in silico investigations of coumarin-based thiazoles, Journal of Medicinal Chemistry, 67 (2024) 7406-7430.

[3] H.O. Tawfik, A. Petreni, C.T. Supuran, M.H. El-Hamamsy, Discovery of new carbonic anhydrase IX inhibitors as anticancer agents by toning the hydrophobic and hydrophilic rims of the active site to encounter the dual-tail approach, European Journal of Medicinal Chemistry, 232 (2022) 1-21.

[4] H.O. Tawfik, M.A. Shaldam, A. Nocentini, R. Salem, H. Almahli, S.T. Al-Rashood, C.T. Supuran, W.M. Eldehna, Novel 3-(6-methylpyridin-2-yl)coumarin-based chalcones as selective inhibitors of cancer-related carbonic anhydrases IX and XII endowed with anti-proliferative activity, J. Enzyme Inhib. Med. Chem., 37 (2022) 1043-1052.

[5] M.A. Abdelrahman, H.S. Ibrahim, A. Nocentini, W.M. Eldehna, A. Bonardi, H.A. Abdel-Aziz, P. Gratteri, S.M. Abou-Seri, C.T. Supuran, Novel 3-substituted coumarins as selective human carbonic anhydrase IX and XII inhibitors: Synthesis, biological and molecular dynamics analysis, Eur. J. Med. Chem., 209 (2021) 112897.

[6] M. Fares, W.M. Eldehna, S. Bua, C. Lanzi, L. Lucarini, E. Masini, T.S. Peat, H.A. Abdel-Aziz, A. Nocentini, P.A. Keller, C.T. Supuran, Discovery of Potent Dual-Tailed Benzenesulfonamide Inhibitors of Human Carbonic Anhydrases Implicated in Glaucoma and in Vivo Profiling of Their Intraocular Pressure-Lowering Action, J. Med. Chem., 63 (2020) 3317-3326.

[7] A.E. Elsawi, M.M. Elbadawi, A. Nocentini, H. Almahli, S. Giovannuzzi, M. Shaldam, R. Salem, T.M. Ibrahim, H.A. Abdel-Aziz, C.T. Supuran, W.M. Eldehna, 1,5-Diaryl-1,2,4-

triazole Ureas as New SLC-0111 Analogues Endowed with Dual Carbonic Anhydrase and VEGFR-2 Inhibitory Activities, J. Med. Chem., 66 (2023) 10558-10578.

[8] W.M. Eldehna, M. Fares, A. Bonardi, M. Avgenikos, F. Baselious, M. Schmidt, T. Al-Warhi, H.A. Abdel-Aziz, R. Rennert, T.S. Peat, C.T. Supuran, L.A. Wessjohann, H.S. Ibrahim, 4-(Pyrazolyl)benzenesulfonamide Ureas as Carbonic Anhydrases Inhibitors and Hypoxia-Mediated Chemo-Sensitizing Agents in Colorectal Cancer Cells, J. Med. Chem., 67 (2024) 20438-20454.

[9] H.S. Salam, M.M. Tawfik, M.R. Elnagar, H.A. Mohammed, M.A. Zarka, N.S. Awad, Potential apoptotic activities of Hylocereus undatus peel and pulp extracts in MCF-7 and Caco-2 cancer cell lines, Plants, 11 (2022) 2192.

[10] M.J. Ahsan, J.G. Samy, H. Khalilullah, M.S. Nomani, P. Saraswat, R. Gaur, A. Singh, Molecular properties prediction and synthesis of novel 1,3,4-oxadiazole analogues as potent antimicrobial and antitubercular agents, Bioorganic and Medicinal Chemistry Letters, 21 (2011) 7246-7250.

[11] N.C. Desai, G.M. Kotadiya, K.A. Jadeja, K.N. Shah, A.H. Malani, V. Manga, T. Vani, Synthesis, antitubercular, antimicrobial activities and molecular docking study of quinoline bearing dihydropyrimidines, Bioorganic Chemistry, 115 (2021) 1-14.